ARECIBO MULTI-FREQUENCY TIME-ALIGNED PULSAR AVERAGE-PROFILE AND POLARIZATION DATABASE

Timothy H. Hankins
Physics Department, New Mexico Tech
Socorro, NM 87801
thankins@nrao.edu

AND

Joanna M. Rankin
Physics Department, University of Vermont
Burlington, VT 05401
Joanna.Rankin@uvm.edu
Draft version December 10, 2008

ABSTRACT

We present Arecibo time-aligned, total intensity profiles for 46 pulsars over an unusually wide range of radio frequencies and multi-frequency, polarization-angle density diagrams and/or polarization profiles for 58 pulsars pulsars at some or all of the frequencies 50, 111/130, 430 and 1400 MHz. The frequency-dependent dispersion delay has been removed In order to align the profiles for study of their spectral evolution and wherever possible the profiles of each pulsar are displayed on the same longitude scale. Most of the pulsars within Arecibo's declination range that are sufficiently bright for such spectral or single pulse analysis are included in this survey—and the calibrated pulse sequences are available by web download for further study.

Subject headings: pulsars:general — polarization

1. INTRODUCTION

As part of a program to study the geometrical constraints on the emission mechanism of pulsars, we have recorded a set of total intensity average profiles at a number of frequencies from 25 to 4800 MHz at the Arecibo Observatory. The data were time-tagged so that through use of a suitable timing model for the pulsar, we were able to shift the arrival times of the pulses, modulo one stellar rotation period, to the solar system barycenter. Then by assuming a dispersion measure DM, we shifted all the profiles to infinite frequency arrival time. In many cases the dispersion measure was the only free parameter for alignment. The techniques used were similar to those of Hankins & Rickett (1986). **In a few cases our observations were coordinated with others made at the Pushchino Radio Astronomy Observatory (PRAO; Hankins** *et al.* **1991).** In addition we have observed a large overlapping group of pulsars at selected frequencies with full Stokes' parameters. We present these two sets of observations in a coordinated fashion, so that they can be used for studies of the pulsar magnetospheric structure. In several cases, where this polarimetry was incomplete, we have included profiles from older polarimetric observations.

Here we present these observations using three different kinds of analysis in order to introduce them to the pulsar community as a resource for future scientific use. They are available for download at http://www.uvm.edu/pulsar.

All three types of analysis and display have a long history at the Arecibo Observatory. As mentioned above, Hankins & Rickett (1986) pioneered this technique, and a further independent effort was made by Phillips & Wolszczan (1992). Programs of both average profile and in-

dividual pulse polarimetry using single channels began in 1971 at 430 MHz (*e.g.,*, Rankin *et al.* 1975; Rankin & Benson 1981) and at 21 cms after the first (1972-74) upgrading (Stinebring *et al.* 1984; Rankin *et al.* 1989), paving the way for the more sensitive and better resolved multi-channel observations reported here **as well as the extensive and recent 1400- and 430-MHz polarization compendia by Weisberg** *et al.* **(1999, 2004).** Stinebring *et al.*, in particular, solved the vexing problem of correcting for cross-coupling errors in the polarimetry (see also, the Appendix below). Finally, we display the polarimetry in two different ways: for weaker pulsars we give their average Stokes profiles, but for stronger ones we compute polarization-angle (hereafter PA) density displays similar in concept to those first presented by Backer & Rankin (1980).

Profile polarimetry programs, of course, have been carried out at other pulsar observatories: *e.g.,*, Jodrell Bank (*e.g.,*, Lyne *et al.* 1971; Gould & Lyne 1998); NRAO 300-ft (*e.g.,*, Manchester 1971); Parkes (Hamilton *et al.* 1977; McCulloch *et al.* 1978; Manchester *et al.* 1980; Johnston *et al.* 2006); Effelsberg (*e.g.,*, Morris *et al.* /1981; von Hoensbroech & Xilouris 1997); Pushchino (*e.g.,*, Suleimanova & Pugachev 2002) **and most recently the GMRT (***e.g.,***, Johnston** *et al.* **2008)**— and many of these observations have been deposited for download at the European Pulsar Network web site (http://www.mpifr-bonn.mpg.de/div/pulsar/data). However, within its declination range, Arecibo's great sensitivity is often highly advantageous, especially for individual pulse polarimetry, although the GMRT in India now achieves comparable sensitivity at some frequencies (*e.g.,*, Mitra *et al.* 2007; **Johnston** *et al.* **2008).**

2. OBSERVATIONS

The results of two main programs of time-aligned total-power and polarimetric pulse-sequence observations presented below were made at the Arecibo Observatory during a number of sessions between 1988 and 1992. A few observations from a previous polarimetric pulse-sequence survey at 430 MHz (Rankin & Campbell, unpublished; hereafter RC) and a subsequent one at 21 cm (Stinebring *et al.* 1984; hereafter SCRWB), however, are also included in order to extend the completeness of our coverage.[1]

2.1. *Multiple frequency total intensity profiles*

For the total intensity observation program, circularly polarized feeds were used at 430, 1400, 2370, and 4800 MHz and crossed-dipole linearly polarized feeds (with circular hybrids) were used at 130/111, 49, and 26 MHz. All profiles were obtained using the then existing Arecibo 40-MHz Correlator (Hagen 1987); the autocorrelation functions (ACFs) were accumulated into typically 1024 pulsar-synchronous phase bins spanning one pulsar period, and then dumped to tape every two minutes.

These ACFs were then Fourier transformed off-line to obtain power spectra, and the appropriate dispersion delays between adjacent spectral channels were removed. The profiles from all spectral channels were then co-added to produce a dedispersed average profile. The two-minute averages were edited to remove interference and other corruption, then synchronously added together to form (in many cases) a high-signal-to-noise ratio (hereafter S/N) average profile. The time-tag of the first sample was used to relate the times of arrival to the solar system barycenter in terms of the pulsar phase at infinite frequency. Thus if the dispersion delays strictly obey the cold plasma dispersion law, then the pulses align in pulse phase exactly as they would if the observer were in the immediate pulsar neighborhood. The dispersion measure *DM* is, however, a free parameter in the phase alignment, and we found that adjustments from the tabulated values (Taylor, Manchester & Lyne 1993, Manchester 2002) were required for optimal alignment for many of the pulsars. The dispersion measures and timing models used for alignment are listed in Table 1.

To test and monitor the timing stability of the system during each observing session, we recorded a reference profile from a strong pulsar using the same sampling parameters each time. From these profiles systematic timing offsets could be determined and applied to data from other pulsars. Since it was not possible to observe throughout the whole range of frequencies in a single observing session, we recorded reference profiles for each pulsar, usually at 430 MHz, to confirm its tabulated timing model. In a number of cases we had to make minor adjustments in the timing model to achieve alignments among profiles recorded at the same frequency; **where applicable, these are indicated in the Notes of Table 4**. After any timing issues were resolved, the dispersion measure was adjusted to obtain pulse-phase alignment among profiles at different frequencies. Since the change in pulse phase ϕ as a function of radio frequency ν, $d\phi/d\nu \propto \nu^{-3}$, we used the lowest frequency pairs with good S/N to determine any adjustment to *DM*.

The fiducial point of a pulse profile to be used for interfrequency alignment depends upon the pulse shape. Usually aligning core components works well for pulsars with odd numbers of components. We aligned either the peak of the core component or the (symmetrical) half-power points for these pulsars. For double profiles, where the separation between the main components is clearly frequency dependent, we used the centroid between the two components.

2.2. *Polarimetry*

Most of the primary polarimetry observations were carried out during a set of sessions in October 1992; a few, however, come from earlier observations in March 1992 and January 1990. All used the then existing Arecibo 40-MHz Correlator, such that the average polarimetry was carried out in a continuous mode, whereas the pulse-sequence observations entailed use of special programs which gated the correlator synchronously with the pulsar. In both cases the basic data recorded at the telescope were the auto- and cross-correlation functions of the left- and right-hand channel voltages. The 21-cm observations used a 20-MHz bandwidth and the lower a maximum of 10-MHz at 430 MHz, 2.5 MHz at 111/130 MHz, and 625 kHz at 49 MHz. A minimum of 32 correlation lags were retained in order to reduce the dispersion delay across the bandpass to usually negligible levels. The resolution was then often essentially the correlator dump time for the pulse-sequence observations and the averaging-bin size for the profile-polarization measurements. These parameters are tabulated in Table 2. The Arecibo 40-MHz Correlator is described by Hagen (1987) and the continuous and gated observing software by Perillat (1988, 1992). The measured correlation functions were scaled, 3-level-sampling corrected, and Fourier transformed to produce raw Stokes parameters, which were in turn corrected (channel by channel) for dispersion, Faraday rotation, instrumental delays, and all of the known feed imperfections as determined by full-sky tracks of pulsar B1929+10 and other sources. These methods are more completely described in the Appendix. During the course of our analyses, we discovered that the instrumental polarization is highly frequency dependent, particularly at 430 MHz; therefore, the most recent observations represent some of the best calibrated ever made at the Arecibo Observatory. For some few, however, not all of the calibration information was available for one reason or another. We found, for instance, that interference rather easily corrupted our continuum-source observations, which are needed to determine the relative left- and right-hand channel gains, so as to calibrate the circular polarization V. In any case, Table 2 indicates this gain calibration with a "c" when a continuum source was used and and "n" when computed from the off-pulse noise level. The correction of the Stokes parameters for cross-coupling in the feed is denoted by a "p".

Profile and single-pulse polarimetry were also carried out during these three sessions at 111.5/130 MHz and near 50 MHz. The techniques were virtually identical to

---

[1] The first two programs were approved under the Arecibo project numbers P868 and P1260 and the latter two as P110 and P467, respectively. Users of these observations must bear in mind that the programs have different data formats.

those described above except that additional corrections were required for the changing ionospheric Faraday rotation and many fewer of our efforts to obtain reliable feed cross-coupling data were successful.

The older 430-MHz observations were carried out in the early 1970s with a single-channel polarimeter using various bandwidths and integration times as indicated by the particular star being observed; these are tabulated in Table 2. The polarimetry scheme is described in Rankin *et al.* (1975); and while the nominal 0.25% voltage amplitude of the feed crosscoupling—which can produce spurious circular polarization at typical levels of about 10% of the linear polarization—was known from radar observations, correction of the Stokes parameters was then impossible because the cross-coupling phase was unknown.

The older 1400-MHz observations were carried out in October 1981, again with a single-channel, adding polarimeter. Here, the bandwidths ranged up to 40 MHz, with these and the integration times chosen to provide a resolution of about a milliperiod. A serious effort was made for the first time to correct the measured Stokes parameters for instrumental cross-coupling distortion using the "orthogonal" approximation described by Stinebring *et al.* (1984).

In all cases we make no effort to give absolute polarization position angles. Therefore, the position angles in our polarization displays are arbitrary within a constant value.

Generally, our polarimetric analyses used the then existing tabulated rotation measures on the ATNF website (Manchester 2002; url-http://www.atnf.csiro.au/research/pulsar/psrcat/). However, in a few cases we were able to measure new rotation measures where they were then unknown. These were determined in the course of our polarimetric analyses by fitting the polarization position-angle swing across the available bandwidth. The errors in the rotation-measure values were computed from the position-angle errors which in turn were computed from the off-pulse noise level and represent one standard deviation. The values are given in boldface with their errors in Tables 1 & 2. The value for B1919+14 remains a new determination, whereas the other f ive generally agree with values determined since within their errors. No effort was made to correct for the effect of ionospheric Faraday rotation, either on the estimated errors of measured rotation measures or in the processing using the tabulated interstellar values; however, at Arecibo this contribution typically no larger than ± 1 rad-m^2, thus well within the stated errors.

3. RESULTS

Our results are summarized in the tables and figures. Table 1 gives the period, period derivative, timing epoch and dispersion-measure value used for the multi-frequency alignments, and Tables 2 & 3 give the observations date, configuration, resolution and rotation-measure value used in the polarimetric analyses. Comments on Tables 1 & 2 are given in Table 4.

The combined multi-frequency and polarimetry results are presented in approximate Right Ascension order in Figures 1 through 17 in order to facilitate intercomparison. The multi-frequency profiles are normally positioned in the lefthhand columns and the 430- and 1400-MHz polarization displays in the central (C) and righthand (R) columns, where they are available—and in the half-dozen cases where both 111/130- and 50-MHz polarimetry is also available, these are given in the center and righthand columns of the following row. Details of the multifrequency alignments and polarimetry are given in Tables 1 & 2. In several cases where no polarimetry was available, the multi-frequency results are interpolated into the sequence (Fig. 8 (top row), Fig. 10 center row, and Fig. 11 bottom left). Finally, Figures 18-19 give polarimetry results for those stars where only single-frequency observations were carried out, and these in turn are described in Table 3. The time resolution of the multifrequency profiles is indicated by a set of three horizontal bars plotted on the left side of the profiles. The upper bar denotes the phase shift which would result from a change of dispersion measure of 0.01, 0.1, or 1.0 pc cm^{-3}. The middle bar, labeled "BW" shows the time resolution limited by the dispersion sweep time, $\tau_{DM} = DM\Delta\nu/(1.205 \times 10^{-16}\nu^3)$, across the receiver bandwidth, $\Delta\nu$, tuned to frequency ν. The bottom bar shows the integration time constant used for the plot. On the left side of the multifrequency profile plots an error bar is plotted to show the range of 2 standard deviations of the off-pulse noise level.

For the polarization plots the total intensity, linear and circular polarizations are depicted by solid, dashed and dotted lines, respectively. The solid vertical bars indicate the range of 3 standard deviations of the off-pulse noise. Where present, the time resolution, including the effects of dispersion across the receiver band and the post integration time constant are shown by a horizontal bar. In the lower part of each polarization plot the average linear polarization position angle is shown wherever the linear polarization exceeds two times the off-pulse noise level.

Error bars for the position angle are shown for $\pm 3\sigma$ uncertainties due to the estimation error of the linear polarization. For many of the pulsars individual pulse records were available. For these pulsars the position angle of each sample which exceeded 2 times the off-pulse noise is plotted as a dot. This type of plot allows study of polarization moding behavior (Manchester, Taylor & Huguenin 1975, Backer & Rankin 1980).

4. DOWNLOADS

Data files corresponding to the pulse sequences and profiles presented in this paper are available for download at www.uvm.edu/pulsar along with Fortran 77 codes for reading them. Complete explanations of the data formats are given as comments in these codes. If these observations and codes are used in future publications, we ask that reference be made to this paper.

TABLE 1

ALIGNMENT PERIODS, PERIOD DERIVATIVES, REFERENCE EPOCH, AND DISPERSION MEASURES

Pulsar	P (s)	$\dot{P} \times 10^{-15}$ (s/s)	Epoch (MJD)	DM (pc cm^{-3})	Ephemeris References	Note	Figure
B0301+19	1.3875836665891	1.29613	42325.500	15.650	C,C,C,C	*a.*	1
B0523+11	0.354437595275	0.07362	48382.000	79.294	M,M,M,M		1
B0525+21	3.74549702041	40.0565	41993.500	51.024	C,C,C,C	*b.*	1
B0540+23	0.2459740892957	15.42378	48382.000	77.698	M,M,M,M		2
B0611+22	0.33492505401	59.630	42881.000	96.86	M,M,M,H		2
B0626+24	0.476622653938	1.99705	48382.000	84.216	M,M,M,H	*c.*	2
B0656+14	0.384885025950	55.0134	48423.000	14.02	M,M,M,M	*d.*	3
B0751+32	1.44234944724	1.0802	43830.000	40.04	M,M,M,M	*e.*	3
B0820+02	0.864872751896	0.10366	43419.347	23.6	M,M,M,M	*f.*	3
B0823+26	0.53066061717618	1.714776	47165.705796	19.4750	Mc,Mc,Mc,H		4
B0834+06	1.273768080098	6.7995	48362.00	12.8579	H,M,M,H	*g.*	4
B0919+06	0.43061431085	13.7248	43890.786	27.3091	H,T,T,T	*h.*	5
B0940+16	1.08741772517	0.1	48500.00	20.5	M,M,M,H		5
B0943+10	1.097704890211	3.4884	45781.306	15.339	S,S,S,H	*i.*	6
B0950+08	0.253065180710	0.229314	47165.7973	2.9701	Mc,Mc,Mc,H		6
B1133+16	1.187913314434	3.7341	47177.902	4.8472	Mc,Mc,Mc,H	*j.*	7
B1237+25	1.38244915690	0.95954	47177.91	9.277	Mc,Mc,Mc,H	*k.*	7
B1530+27	1.124835519553	0.803	46387.700	14.67	H,M,M,H		8
B1541+09	0.74844817748	0.43030	42304.00	34.99	T,T,T,T		8
B1604−00	0.4218162717899	0.30610	48419.00	10.6831	H,M,M,H		8
B1612+07	1.2068002120	2.357	43891.065	21.5	M,M,M,M		8*b*
B1633+24	0.490506485351	0.1195	46075.099	24.265	M,M,M,H		8*c*
B1737+13	0.803049715913	1.454	43892.616	48.73	H,M,M,H		9
B1821+05	0.752906449119	0.225	43890.159	66.7827	H,M,M,H		9
B1839+09	0.38131888145508	1.0916	43890.169	49.132	H,M,M,H		9
B1842+14	0.375462510949	1.866	43986.911	41.6	H,M,M,M		10
B1900+01	0.72930163274	4.0322	42345.50	245.	M,M,M,H		10
B1907+00	1.01694545765	5.5151	42647.00	111.	M,M,M,M		10*e*
B1907+03	2.330260471	4.53	43984.933	83.5	M,M,M,H		10*f*
B1915+13	0.19462634149	7.20286	42302.00	94.494	T,T,T,M		11
B1918+19	0.82103460383	0.8952	42577.00	153.48	M,M,M,H		11*g*
B1919+21	1.337301192269	1.34809	40689.95	12.4309	M,M,M,M		11
B1920+21	1.07791915514	8.1899	42547.00	217.1	M,M,M,M		11*i*
B1929+10	0.226517153473	1.15675	41704.00	3.176	H,T,T,T		12
B1933+16	0.358736247894	6.00354	42265.00	158.53	H,M,M,M		12
B1944+17	0.44061846173	0.02404	41501.00	16.11	T,T,T,M		12
B1952+29	0.426676786488	0.00164	48415.00	7.86	M,M,M,H		13
B2016+28	0.557953408114	0.14720	40688.50	14.1965	C,C,C,H	*l.*	14
B2020+28	0.343401720116	1.8935	47018.182	24.623	H,M,M,H		14
B2044+15	1.1382856067	0.185	43890.254	39.71	M,M,M,H		14
B2110+27	1.202851149957	2.6225	46075.294	25.122	H,M,M,H		15
B2113+14	0.440152954660	0.290	43986.016	56.14	H,M,M,H		15
B2210+29	1.00459237450	0.4948	46074.83	74.6	M,M,M,H		16
B2303+30	1.575884744270	2.89567	42341.00	49.575	M,M,M,H	*m.*	16
B2315+21	1.444652673768	1.05	43987.099	20.865	H,M,M,H	*n.*	17

References. — C: Cordes, 1992, H: this work, M: Manchester, *et al.* 2002, Mc: McKinnon, 1990, T: Taylor, *et al.* 1993, S: Shibanova (1990)

Table 2

Polarimetry Configuration, Calibration & Rotation Measure Information for the Results in the Center (C)
and Right (R) Columns Below

Pulsar	Date C	Date R	Config C (MHz/ch)	Config R (MHz/ch)	Resol C (deg)	Resol R (deg)	RM[a] (rad-m^2)	Note	Figure
B0301+19	05/01/74	20/10/92	2./1:c	20./32:cp	0.85	0.31	−8.3		1
B0523+11	17/10/92	20/10/92	1.25/32:cp	20./32:cp	0.41	0.41	78.7		1
B0525+21	01/04/74	11/10/81	2./1:c	20./1:cp	2.76	0.15	50.96		1
B0540+23	05/01/74	20/10/92	0.1/1:c	20./32:cp	1.19	0.38	77.58		2
B0611+22	19/10/92	20/10/92	5./32:cp	20./32:cp	0.85	0.38	67.		2
B0626+24	16/02/92	20/10/92	10./64:cp	20./32:cp	1.06	0.31	82.		2
B0656+14	12/02/92	17/02/92	10./32:cp	20./32:cp	0.43	0.37	22.		3
B0751+32	19/10/92	—	10./32:cp	—	0.32	—	−7.		3
B0820+02	19/10/92	20/10/92	10./32:cp	20./32:cp	0.36	0.36	13.		3
B0823+26	20/10/92	15/10/92	10./32:cp	20./32:cp	0.43	0.34	5.9		4
B0834+06	01/04/74	10/10/81	2./1:c	20./1:cp	0.76	0.22	3.9		4
	16/02/92	03/01/00	0.63/256:n	2.5/128:n	0.70	0.70		*1.*	4
B0919+06	20/10/92	11/10/81	10./32:cp	20./1:cp	0.74	0.68	27.25		5
	17/02/92	15/02/92	0.31/256:n	2.5/128:n	2.00	1.61		*1.*	5
B0940+16	17/10/92	—	10./32:cp	—	0.35	—	53.		5
B0943+10	17/01/00	19/10/92	2.5/64:	10./32:cp	1.18	0.33	13.3	*1.*	6
B0950+08	06/11/71	10/10/81	10./1:c	20./1:cp	0.88	0.28	2.969		6
	15/02/92	—	0.63/128:n	???:	1.99	—		*1.*	6
B1133+16	19/10/92	16/10/92	10./32:cp	20./32:cp	0.31	0.37	3.9		7
	16/02/92	17/01/90	0.63/128:n	1.25/128:n	0.50	0.70		*1.*	7
B1237+25	06/01/74	11/10/81	2./1:c	20./1:cp	0.50	0.10	9.296		7
	—	15/02/92	—	2.5/64:	—	0.35		*1,2.*	7d
B1541+09	14/02/92	17/01/00	2.5/256:	10./32:cp	1.15	1.45	21.	*1.*	8
B1604−00	14/02/92	11/02/73	2.5/128:	10./1:c	1.20	1.91	6.5	*1.*	8
B1737+13	20/10/92	24/10/92	10./32:cp	20./32:cp	0.71	0.36	73.		9
B1821+05	05/01/00	19/10/92	5./64:cp	20./32:cp	0.34	0.36	145.		9
B1839+09	—	23/10/92	—	20./32:cp	—	0.38	53.		9
B1842+14	—	23/10/92	—	20./32:cp	—	0.39	121.		10
B1907+10	21/10/73	24/10/92	0.05/1:c	20./32:cp	0.98	0.51	540.		10
B1915+13	07/09/73	22/10/92	0.1/1:c	20./32:cp	1.82	0.33	233.		11
B1919+21	05/01/00	22/10/92	10./32:cp	20./32:cp	0.19	0.33	−37.		11
B1920+21	—	19/10/92	—	20./32:cp	—	0.34	282.		11
B1929+10	24/12/74	18/10/92	2./1:c	20./32:cp	1.05	0.49	−6.1		12
B1933+16	24/07/73	—	0.1/1:c	—	1.66	—	−1.9		12
B1944+17	27/07/73	23/10/92	2./1:c	20./32:cp	2.78	0.33	−28.		12
B1946+35	08/05/74	18/10/92	0.25/1:c	20./32:cp	1.69	0.35	−78.		13
B1952+29	15/02/00	—	20./32:cp	—	0.35	—	−18.		13
B2002+31	28/07/73	22/10/92	0.25/1:	20./32:cp	1.04	0.34	30.		13
B2016+28	15/10/92	18/10/92	10./32:cp	20./32:cp	0.39	0.39	−34.6		14
B2020+28	16/10/92	18/10/92	10./32:cp	20./32:cp	0.43	0.37	−74.8		14
B2044+15	14/02/92	19/10/92	10./64:cp	20./32:cp	0.40	0.32	−101.		14
B2053+21	20/10/92	18/10/92	10./64:cp	20./32:cp	0.35	0.35	**−100.±7.**		15
B2110+27	14/02/92	22/10/92	10./32:cp	20./32:cp	0.35	0.30	−65.		15
B2113+14	29/10/92	23/10/92	5./32:cp	20./32:cp	0.74	0.37	−25.		15
B2210+29	16/10/92	23/10/92	10./32:cp	20./32:cp	0.43	0.36	**−175.±15.**		16
B2303+30	15/10/92	18/10/92	10./32:cp	20./32:cp	0.37	0.28	−84.		16
	—	22/10/92	—	2.5/128:c	—	0.84		*1.*	16
B2315+21	14/02/92	19/10/92	10./32:cp	20./32:cp	0.35	0.35	−37.		17

[a]The bolded RM values were determined in the course of this work and are given with their estimated errors; whereas the other values were taken from the ATNF pulsar catalog (http://www.atnf.csiro.au/research/pulsar/psrcat/). No effort was made to correct for the ionospheric Faraday rotation, either in processing or in specifying the RM errors, which is typically less that 1 rad-m^2.

TABLE 3
MISCELLANEOUS PULSAR POLARIMETRY DATA (FIGS. 18 & 19).

Pulsar	Date	Config (MHz/ch)	Resol (deg)	RM^{a} (rad-m^2)
B0045+33	16/10/92	10./32:cp	0.40	?
B0609+37	17/10/92	5./32:cp	0.53	8.5
B1845−01	24/10/92	20./32:cp	0.39	580.
B1859+03	18/10/92	20./32:cp	0.66	−237.4
B1900+05	24/10/92	20./32:cp	0.37	−113.
B1910+20	15/02/92	10./64:cp	0.35	148.
B1917+00	08/05/74	0.5/1:c	1.34	—
B1919+14	20/10/92	5./64:cp	0.44	**275.±60.**.
B1923+04	06/01/00	5./32:	0.55	−37.
B1951+32	04/01/00	20./32:cp	2.81	−182.
B2000+32	20/10/92	5./64:cp	1.03	20.
B2028+22	26/10/92	5./64:cp	0.40	**−195.±25.**
B2034+19	26/10/92	10./32:cp	0.35	**−98.5±8.**
B2053+36	24/10/92	20./32:cp	0.66	−68.
B2122+13	16/10/92	10./32:cp	0.51	**−48.3±3.6**

[a]The bolded *RM* values were determined in the course of this work and are given with their estimated errors; whereas the other values were taken from the ATNF pulsar catalog (http://www.atnf.csiro.au/research/pulsar/psrcat/). No effort was made to correct for the ionospheric Faraday rotation, either in processing or in specifying the *RM* errors, which is typically less that 1 rad-m^2.

REFERENCES

Backer, D. C., & Rankin, J. M. 1980, ApJS, 42, 143.
Eilek, J. A., & Hankins, T. H. 2008, ApJ, (in preparation).
Cordes, J. M. 1992, private correspondence.
Gould, D. M., & Lyne, A. G. 1998, MNRAS, 301, 235.
Hagen, J. 1987, NAIC Electronics Department Manual No. 8319.
Hamilton, P. A., McCulloch, P. M., Ables, J. G., & Komesaroff, M. M. 1978, MNRAS, 180, 1
Hankins, T. H., Izvekova, V. A., Malofeev, V. M., Rankin, J. M., Shitov, Yu. P.; Stinebring, D. R. 1991, ApJ, 373, 17.
Hankins, T. H., & Rickett, B. J. 1986 ApJ, 311 684.
von Hoensbroech, A., & Xilouris, K. M. 1997, A&AS, 126, 121.
Johnston, S., Hobbs, G., Vigeland, S., Kramer, M., Weisberg, J. M., & Lyne, A. G. 2006, MNRAS, 364, 1397
Johnston, S., Karastergiou, A., Mitra, D., & Gupta, Y. 2008, MNRAS, 388, 261
Lyne, A. G., Smith, F. G., & Graham, D. A 1971, MNRAS, 153, 377.
Manchester, R. N. 2002, www.atnf.csiro.au/research/pulsar/psrcat
Manchester, R. N. 1971, ApJS, 23, 283.
Manchester, R. N., & Taylor, J. H. & Huguenin, G. R. 1975, ApJ, 86, 418.
Manchester, R. N., & Hamilton, P. A. & McCulloch, P. M. 1980, MNRAS, 192, 153.
Manchester, R. N. 2002, www.atnf.csiro.au/research/pulsar/psrcat
McCulloch, P. M., Hamilton, P. A., Manchester, R. N., & Ables, J. G. 1978, MNRAS, 183, 645.

McKinnon, M. M. 1990, private correspondence.
Mitra, D., Rankin, J. M., & Gupta, Y. 2007, MNRAS, 379, 932
Morris, D., Graham, D. A., Sieber, W., Bartel, N., & Thomasson, P. 1981, A&AS, 46, 421
Perillat, P. 1988, NAIC Computer Department Report No. 23.
Perillat, P. 1992, private communication.
Phillips, J. A. & Wolszczan, A. 1992 ApJ, 385, 273
Rankin, J. M., & Benson, J. M. 1981, AJ, 346, 869
Rankin, J. M., & Campbell, D. B., unpublished (RC)
Rankin, J. M., Campbell, D. B., & Spangler, S. R. 1975, NAIC Report No. 46.
Rankin, J. M., Stinebring, D. R., & Weisberg, J. M. 1989, ApJ, 346, 869
Shabanova, T. V. 1990, Soviet Astr. 34, 269.
Stinebring, D. R., Cordes, J. M., Rankin, J. M., Weisberg, J. M., & Boriakoff, V. 1984, ApJS, 55, 247 (SCRWB)
Suleimanova, S. A., & Pugachev, V. D. 2002, Astronomy Reports, 46, 309
Taylor, J., H., Manchester, R. N., & Lyne, A. G. 1993, ApJS, 88, 529.
Weisberg, J. M., Cordes, J. M., Lundgren, S. C., Dawson, B. R., Despotes, J. T., Morgan, J. J., Weitz, K. A., Zink, E. C., & Backer, D. C. 1999, ApJS, 121, 171 (W-99)
Weisberg, J. M., Cordes, J. M., Kuan, B., Devine, J. E., Green, J. T., & Backer, D. C. 1999, ApJS, 150, 317 (W-04)

The following is a list of the pulsars mentioned to comply with AASTEX§2.15.3. It doesn't print in the right place.
B0045+33 B0301+19 B0523+11 B0525+21 B0540+23 B0609+37 B0611+22 B0626+24 B0656+14 B0751+32 B0820+02 B0823+26 B0834+06 B0919+06 B0940+16 B0943+10 B0950+08 B1133+16 B1237+25 B1530+27 B1541+09 B1604−00 B1612+07 B1633+24 B1737+13 B1821+05 B1839+09 B1842+14 B1859+03 B1900+01 B1900+05 B1907+00 B1907+03 B1907+10 B1910+20 B1915+13 B1918+19 B1917+00 B1919+14 B1919+21 B1920+21 B1923+04 B1929+10 B1933+16 B1944+17 B1946+35 B1951+32 B1952+29 B2000+32 B2002+31 B2016+28 B2020+28 B2028+22 B2034+19 B2044+15 B2053+21 B2053+36 B2110+27 B2113+14 B2122+13 B2210+29 B2303+30 B2315+21

<div align="center">

TABLE 4

NOTES TO TABLES 1 – 2

</div>

Pulsar	Note	
B0301+19	*a.*	2370-MHz profile shifted by −6.17 ms to correct systematic offset; see §2.1.
B0525+21	*b.*	2370-MHz profile shifted by −7.32 ms to correct systematic offset; see §2.1.
B0626+24	*c.*	2370-MHz and 430-MHz profiles shifted by 9.25 and 40.91 ms to correct systematic offset; see §2.1. DM determined from 1408 to 111.5-MHz alignment. The "bump" preceding the 430-MHz pulse at longitude −18° is probably spurious. In a few cases the correlator failed to start at the correct time and thus misaligned certain individual 2-min scans. Most of these faults were corrected at an earlier point in our reduction, but this "bump" was not noticed until after the constituent 2-min scans had been destroyed.
B0656+14	*d.*	430-MHz profile shifted by −11.29 ms to correct systematic offset; see §2.1.
B0751+32	*e.*	Arbitrary alignment by profile centroids; see §2.1.
B0820+02	*f.*	Arbitrary alignment by profile centroids; see §2.1.
B0834+06	*g.*	2370-MHz profile shifted by 8.40 ms to correct systematic offset; see §2.1.
B0919+06	*h.*	4880 and 111.5-MHz profiles shifted by −1.42 and −9.93 ms to correct systematic offsets; see §2.1.
B0943+10	*i.*	The two 111.5-MHz profiles, showing the two modes of B0943+10, were recorded 1 year apart. They align well using Shabanova's (1990) timing model. The 430 and 24.8-MHz profiles, recorded 4 days apart, also align well, so the DM determination is based on this frequency pair. Then these two profiles were shifted by 5.92 ms to align with the 111.5-MHz profiles, and the 49.2-MHz profile is arbitrarily shifted by 26.1 ms to align its centroid.
B1133+16	*j.*	49.2-MHz profile shifted by −9.48 ms to correct systematic offset; see §2.1.
B1237+25	*k.*	4880-MHz profile shifted by 15.1 ms to correct systematic offset; see §2.1.
B2016+28	*l.*	The dramatic pulse shape change between 111.5 and 430 MHz is consistently observed on different days. The DM used for alignment was adjusted to align the 49.2 and 111.5-MHz profile peaks, though if the profile is actually bifurcating at low frequencies, this alignment may be incorrect. We have searched the literature in an effort to see if any other very low frequency profile could settle this bifurcation question, but apparently our 50-MHz observations is the only published profile below 100 MHz.
B2303+30	*m.*	4880 and 1408-MHz profiles shifted by −39.40 ms to correct systematic offset; see §2.1.
B2315+21	*n.*	2370-MHz profile shifted by −37.12 ms to correct systematic offset; see §2.1.
—	*1.*	For the observations at 11/130 MHz and 50 MHz, a search was carried out over a large range of rotation measure to maximize the linear polarization before combining the individual frequency channels, and the successive two-minute scans were rotated to a common polarization angle before combining them. This was found necessary because of a changing effective (ionospheic?) rotation measure with time.
—	*2.*	The 130-MHz polarization display for B1237+25 has been placed in the left column just above the corresponding multifrequency plot.

FIG. 1.— Multi-frequency and polarization displays for B0301+19, B0523+11 and B0525+21. **Usual Figure Layout:** For each pulsar, the multifrequency profiles are given in the left-hand column and the polarimetric displays in the center and right-hand columns, continuing in the row below when more than than two bands are available; occasional departures from this plan will be noted below. **Multifrequency Profiles** are time-aligned (see text) and displayed in ascending-frequency order. Bars are given at the left edge or each profile showing a) the longitude shift corresponding to a particular ΔDM and b) the bandwidth (BW) and integration-time resolutions. **Polarization Histograms** are used to display the individual-pulse polarization properties of B0301+19 and **Polarized Profiles** present the average-polarization observations of B0523+11. Both types of display have two panels with the total power (Stokes I), total linear polarization (L [$=\sqrt{Q^2 + U^2}$]) and circular polarization (Stokes V, given right-hand-left hand) in the upper panel, and the polarization angle (PA [$=\tan^{-1}(U/Q)$]) in the lower one. The **polarization histograms** show the PA density of the individual samples that exceed an appropriate >3 sigma threshold (see text) with the average PA overplotted (red curve). Here, both the total linear (L, dashed red) and circular (V, dotted green) polarization curves are shown in color, and by contrast the polarized profile displays are shown in black and white. In both types of display a small box at the left of the upper panel gives the resolution and a deflection corresponding to two off-pulse noise standard deviations. **Top center credit: RC**
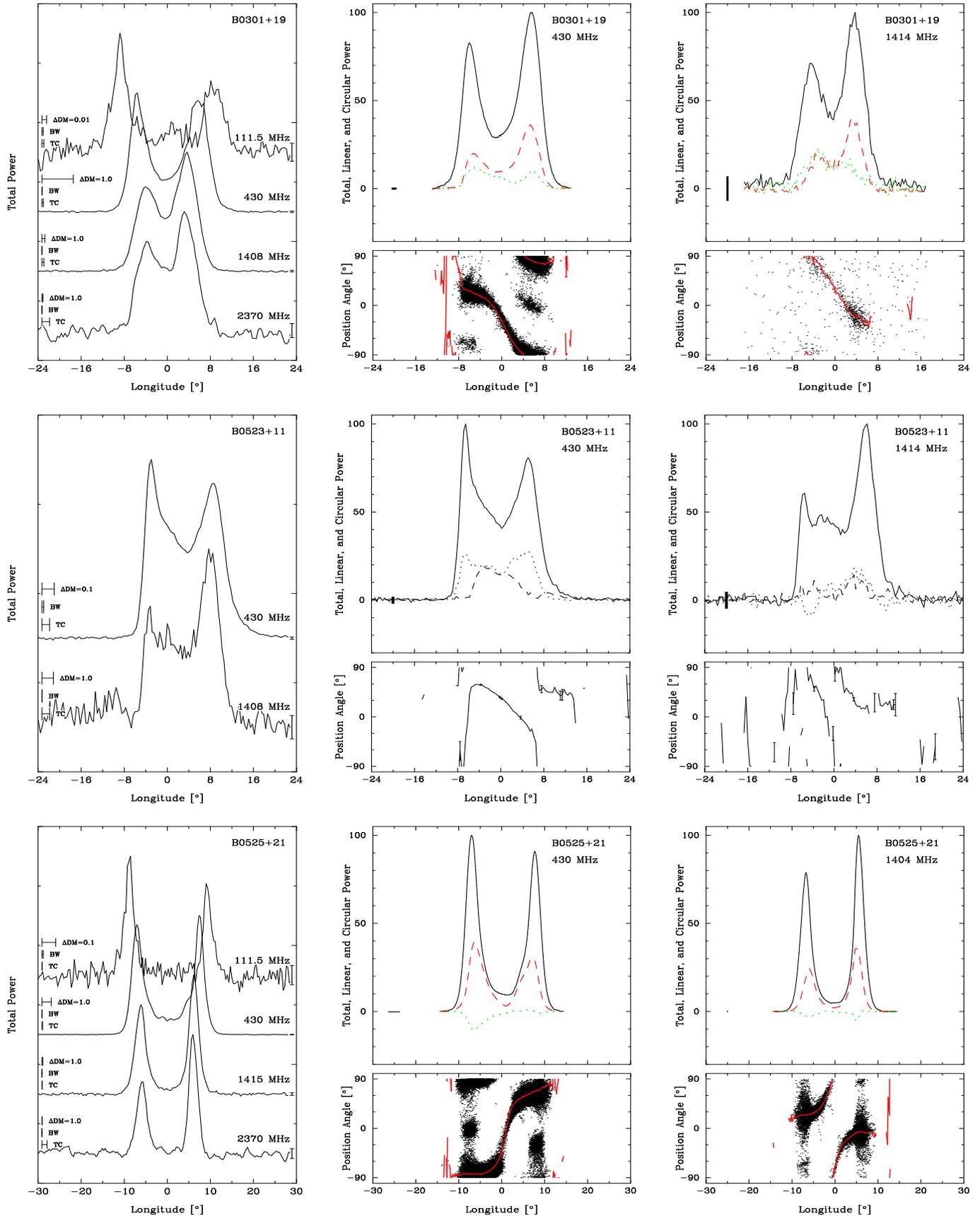
FIG. 1.— See caption, previous page
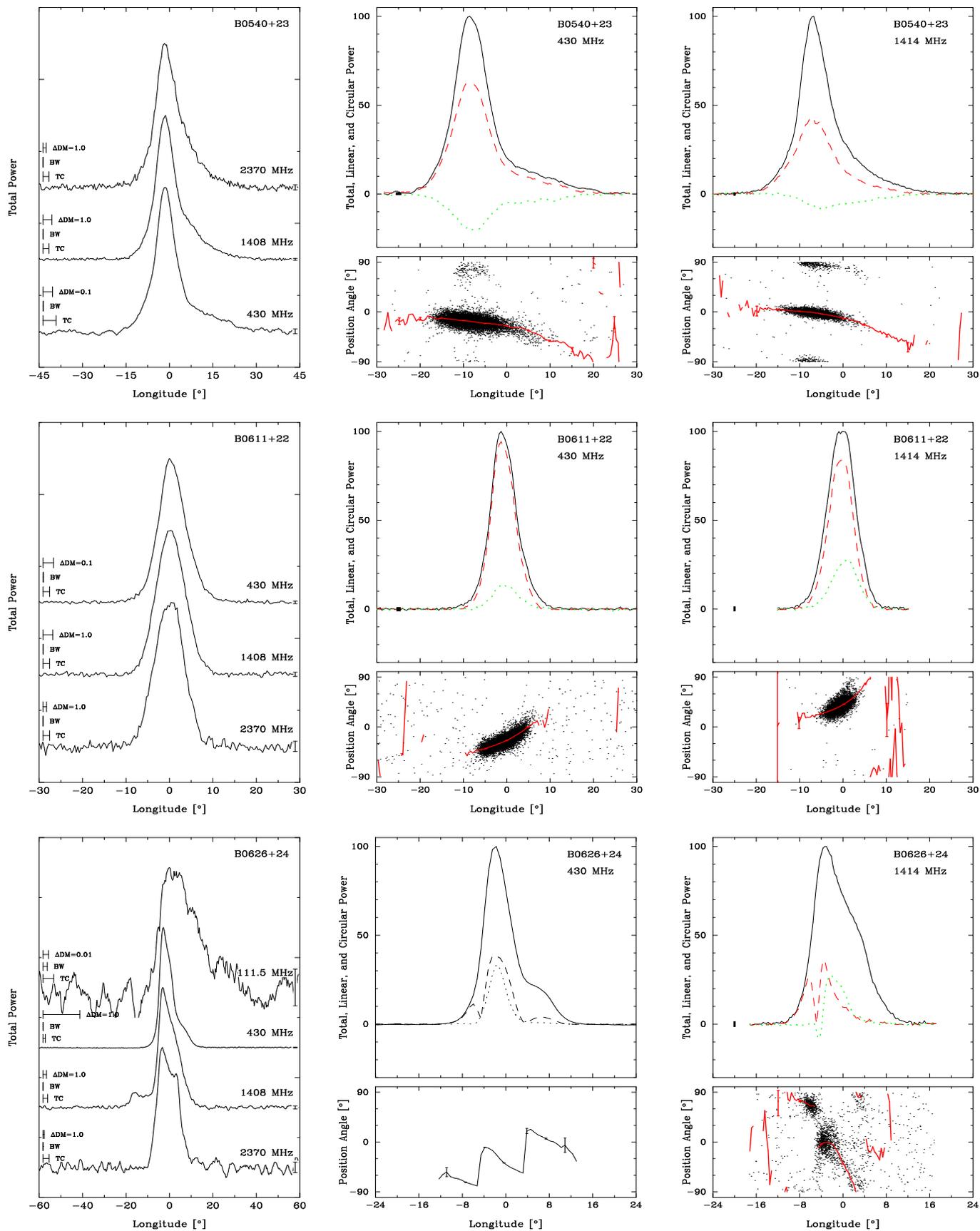
Fig. 2.— Multi-frequency and polarization displays for B0540+23, B0611+22 and B0626+24 as in Fig. 1. **Top center credit: RC**
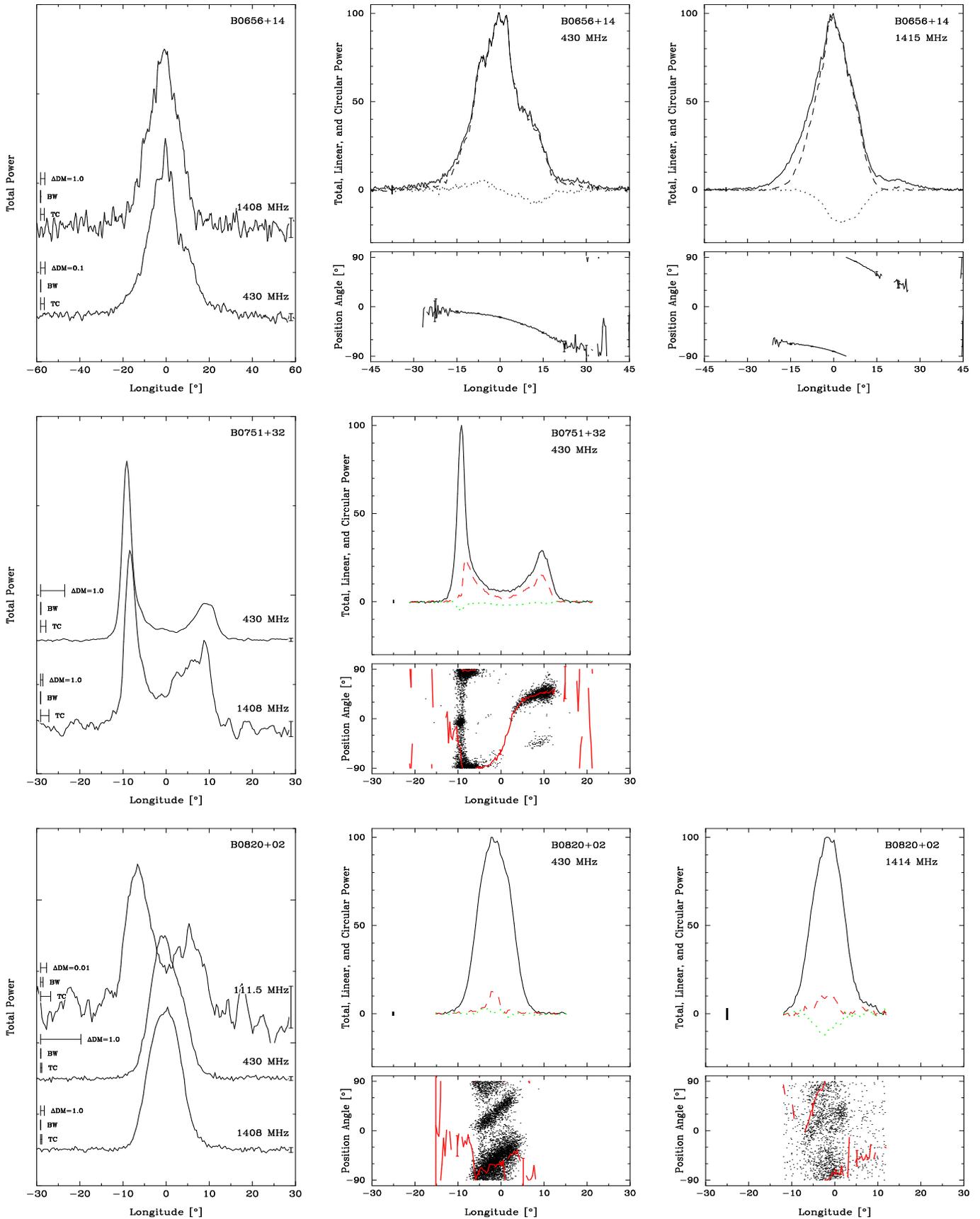
FIG. 3.— Multi-frequency and polarization displays for B0656+14, B0751+32 and B0820+02 as in Fig. 1.
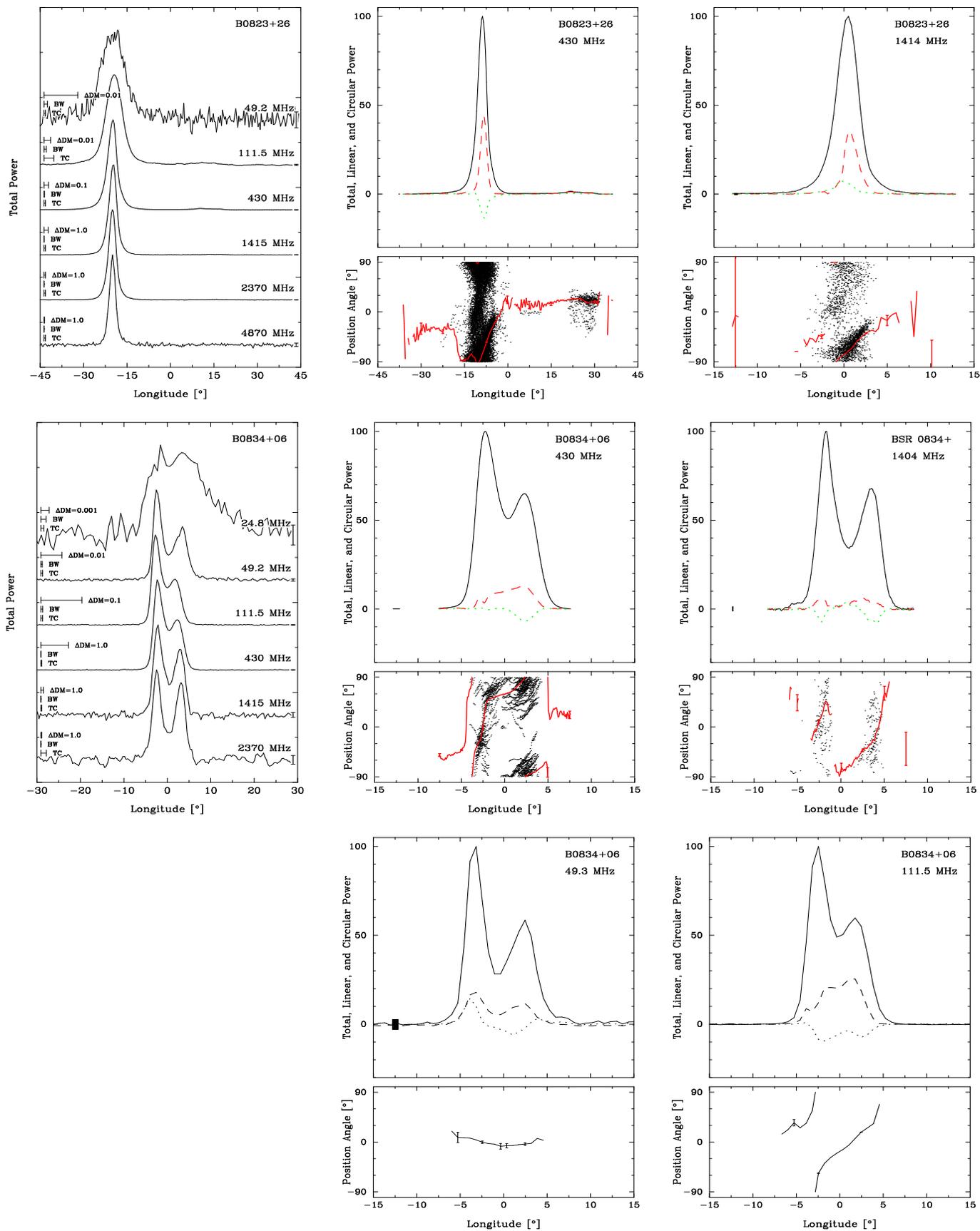
FIG. 4.— Multi-frequency and polarization displays for B0823+26 and B0834+06 as in Fig. 1. **Middle right credit: SCRWB**
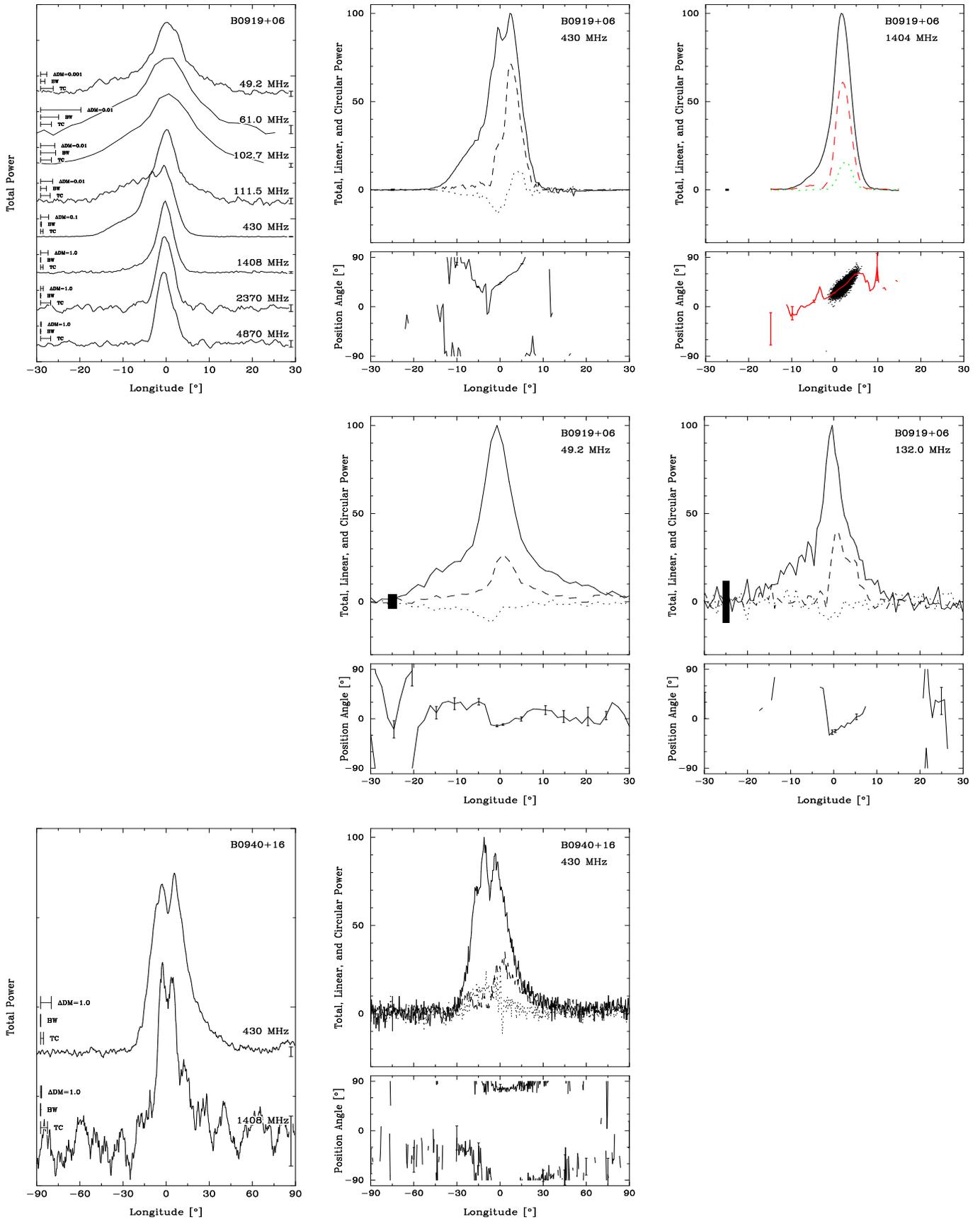
FIG. 5.— Multi-frequency and polarization displays for B0919+06 and B0940+16 as in Fig. 1. The 61- and 103-MHz were coordinated with the Pushchino Observatory (Hankins *et al.* 1991). **Top right credit: SCRWB**
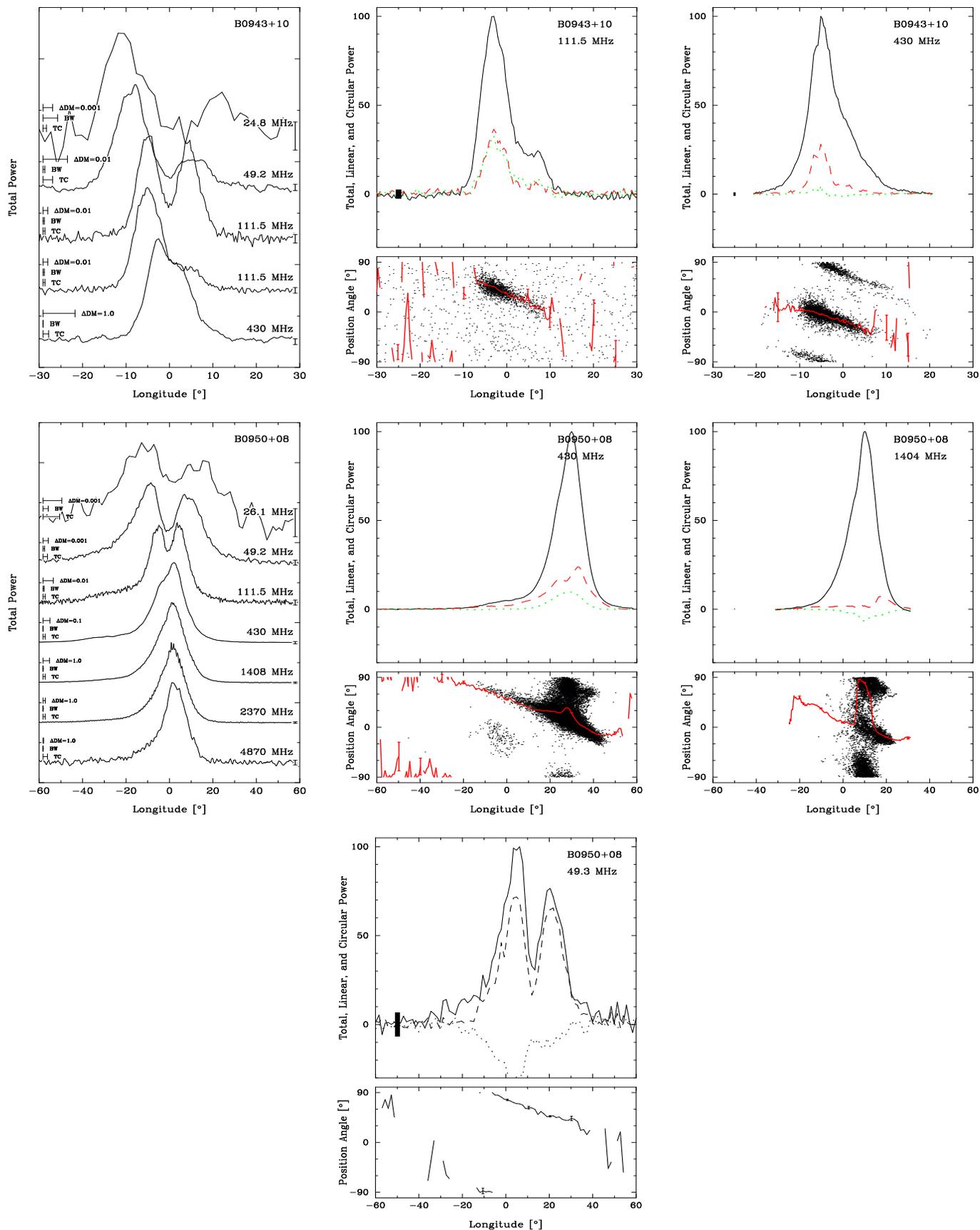
FIG. 6.— Multi-frequency and polarization profiles for B0943+10 and B0950+08 as in Fig. 1. **Middle center and right credits: RC and SCRWB, respectively.**
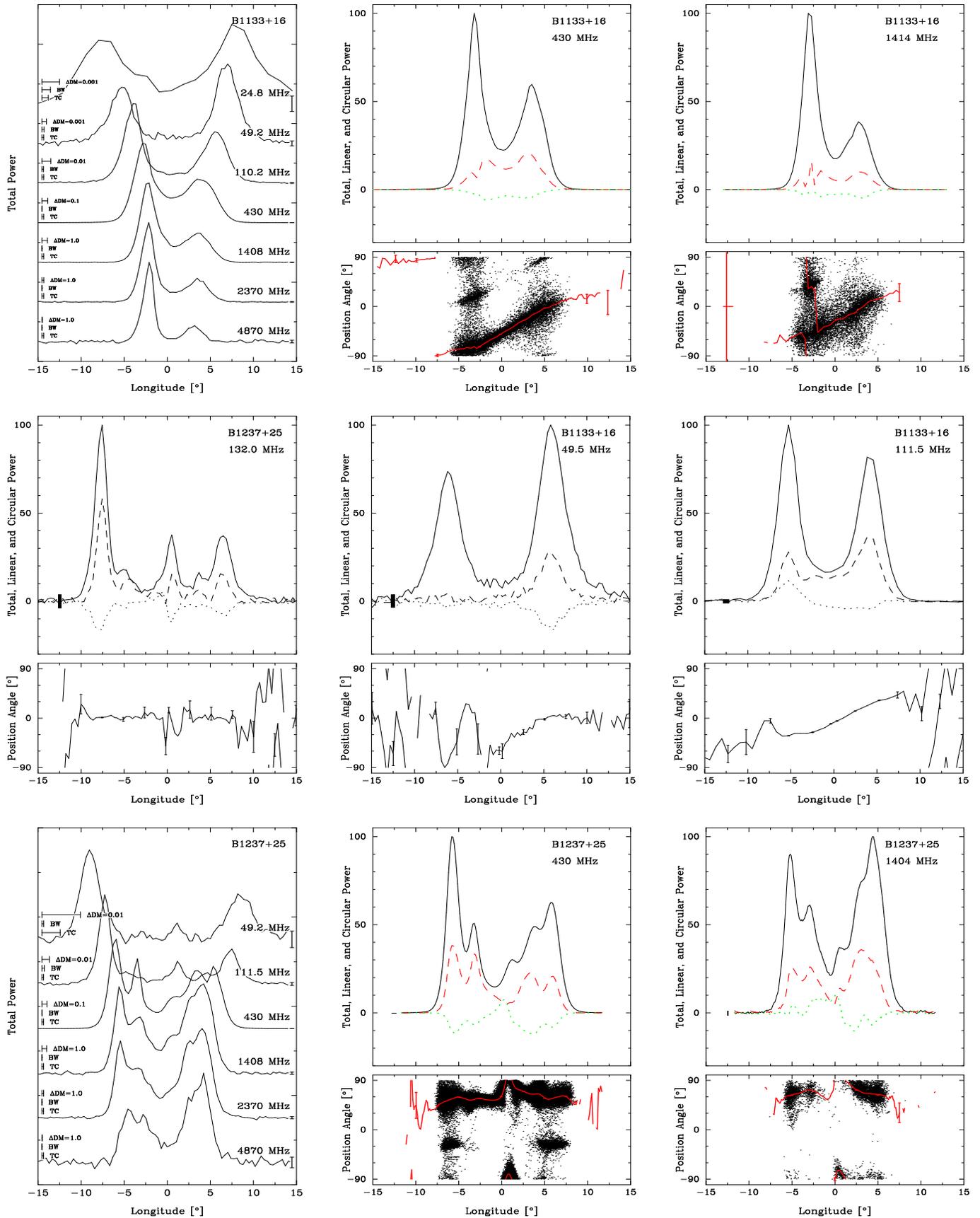
FIG. 7.— Multi-frequency and polarization profiles for B1133+16 and B1237+25 as in Fig. 1. Note the latter's 132-MHz polarization in the center left position. The 110-MHz was coordinated with the Pushchino Observatory (Hankins *et al.* 1991). **Bottom center credit: RC**
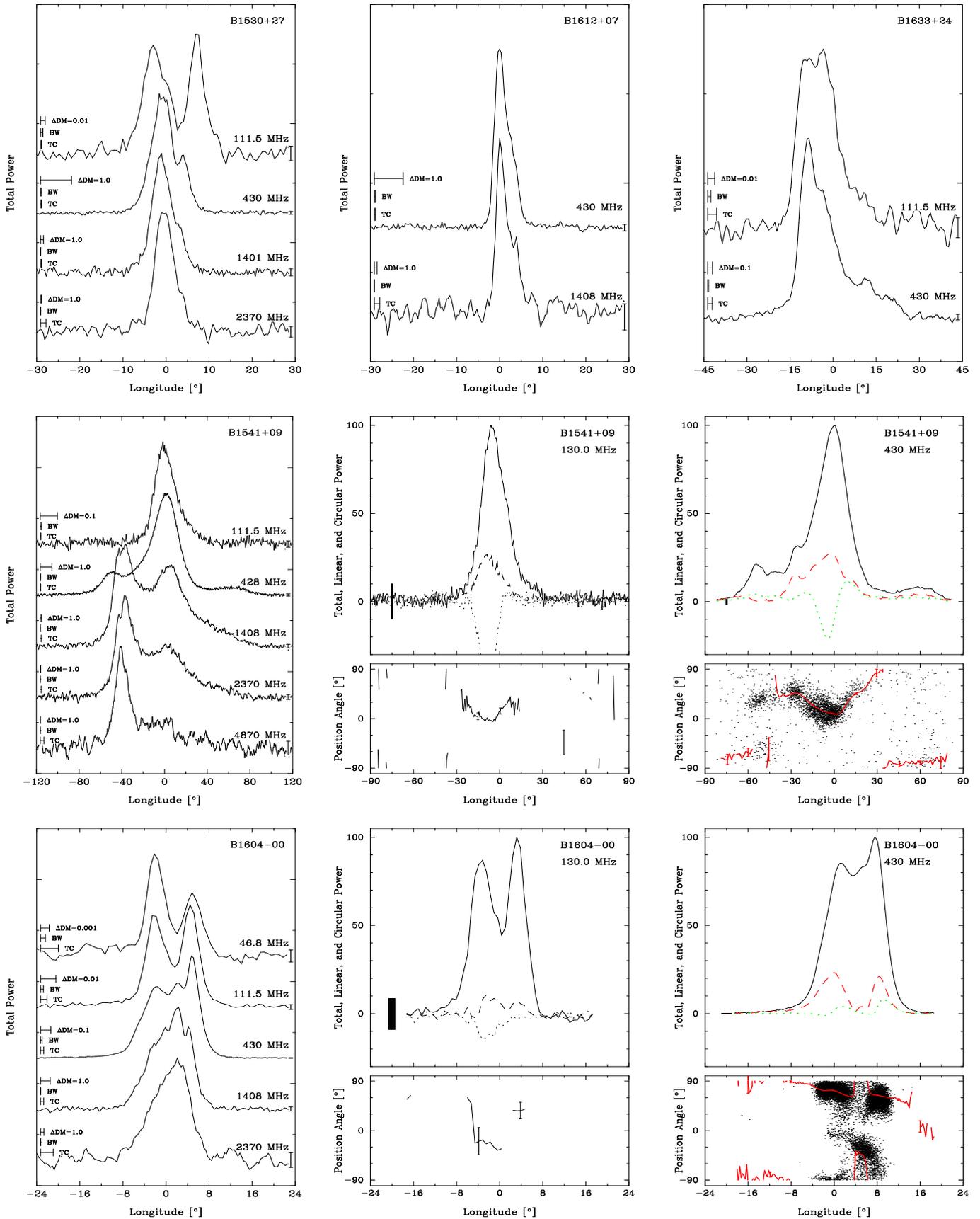
FIG. 8.— Multi-frequency profiles for B1530+27, B1612+07 and B1633+24 are given in the top row . The multi-frequency and polarization displays for B1541+09 and B1604−00 maintain the same layout as in Fig. 1. **Bottom right credit: RC**
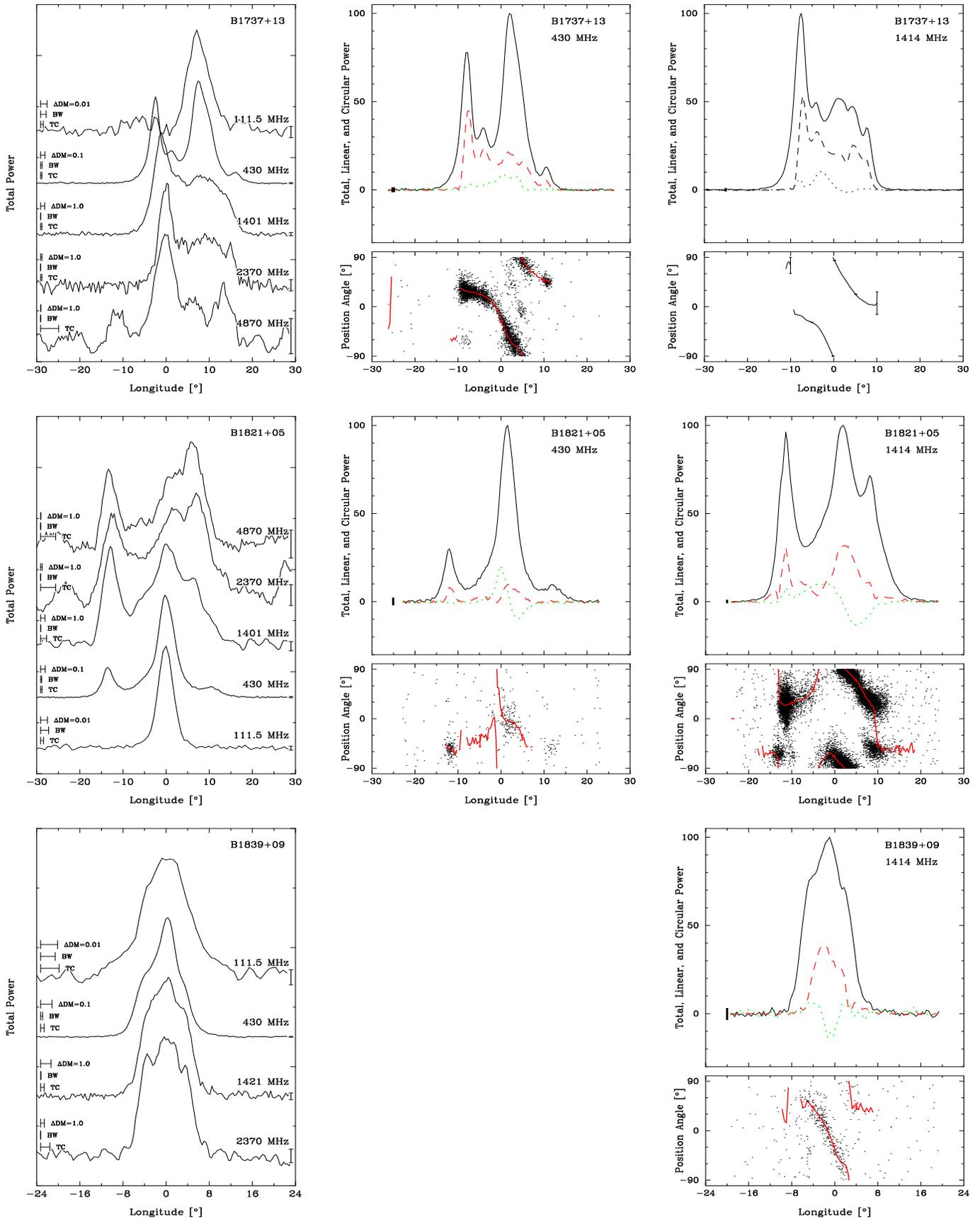
FIG. 9.— Multi-frequency and polarization displays for B1737+13, B1821+05, and B1839+09 as in Fig. 1.
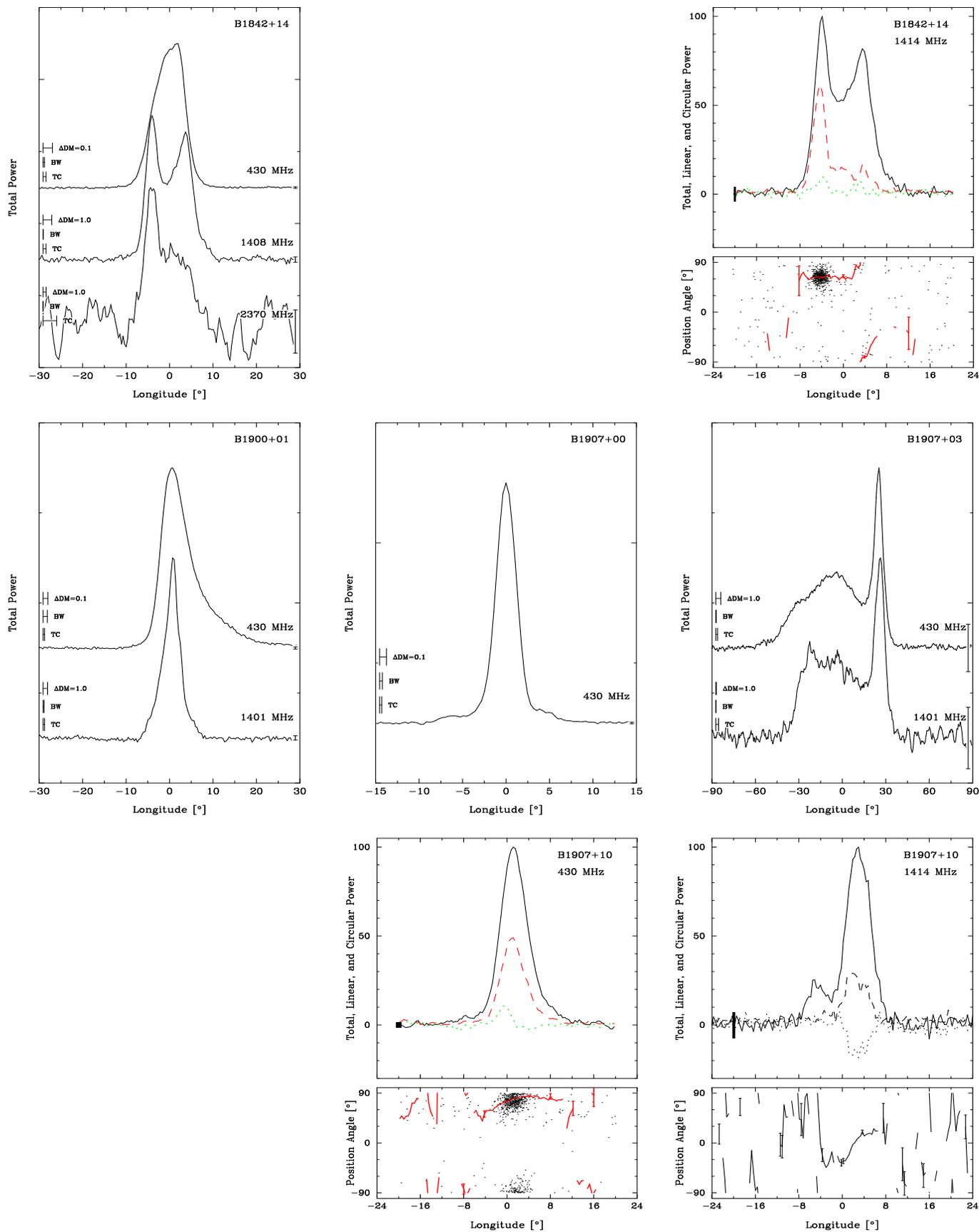
FIG. 10.— Multi-frequency profiles for B1842+14 (top left), B1900+01, B1907+00 and B1907+03 (middle row), and polarization displays for B1842+14 and B1907+10 as in Fig. 1. **Bottom right credit: RC**
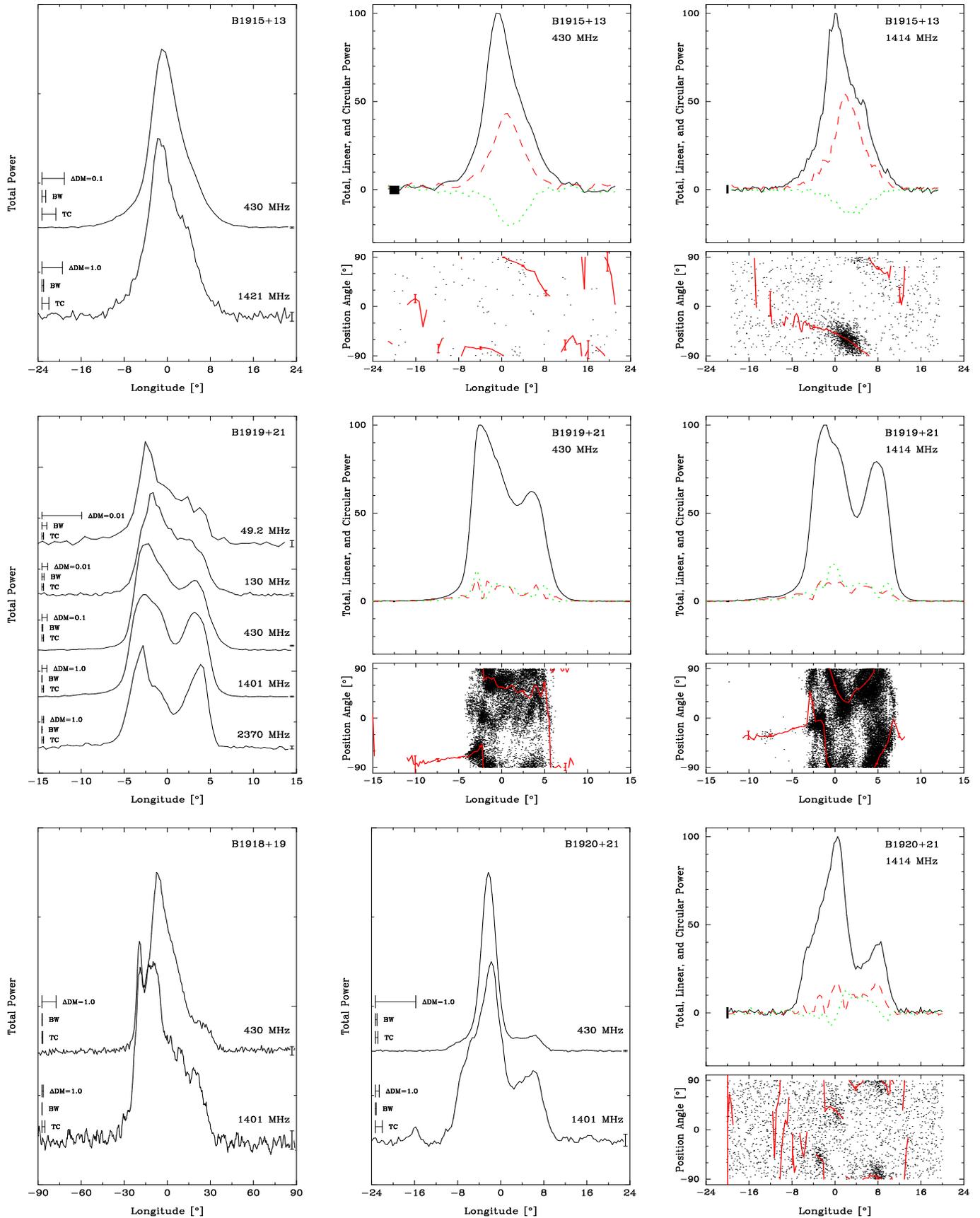
FIG. 11.— Multi-frequency profiles for B1915+13, B1919+21, B1918+19 (bottom left) and B1920+21 (bottom center), and polarization-histogram displays for B1915+13, B1919+21 and B1920+21 as in Fig. 1. **Top center credit: RC**
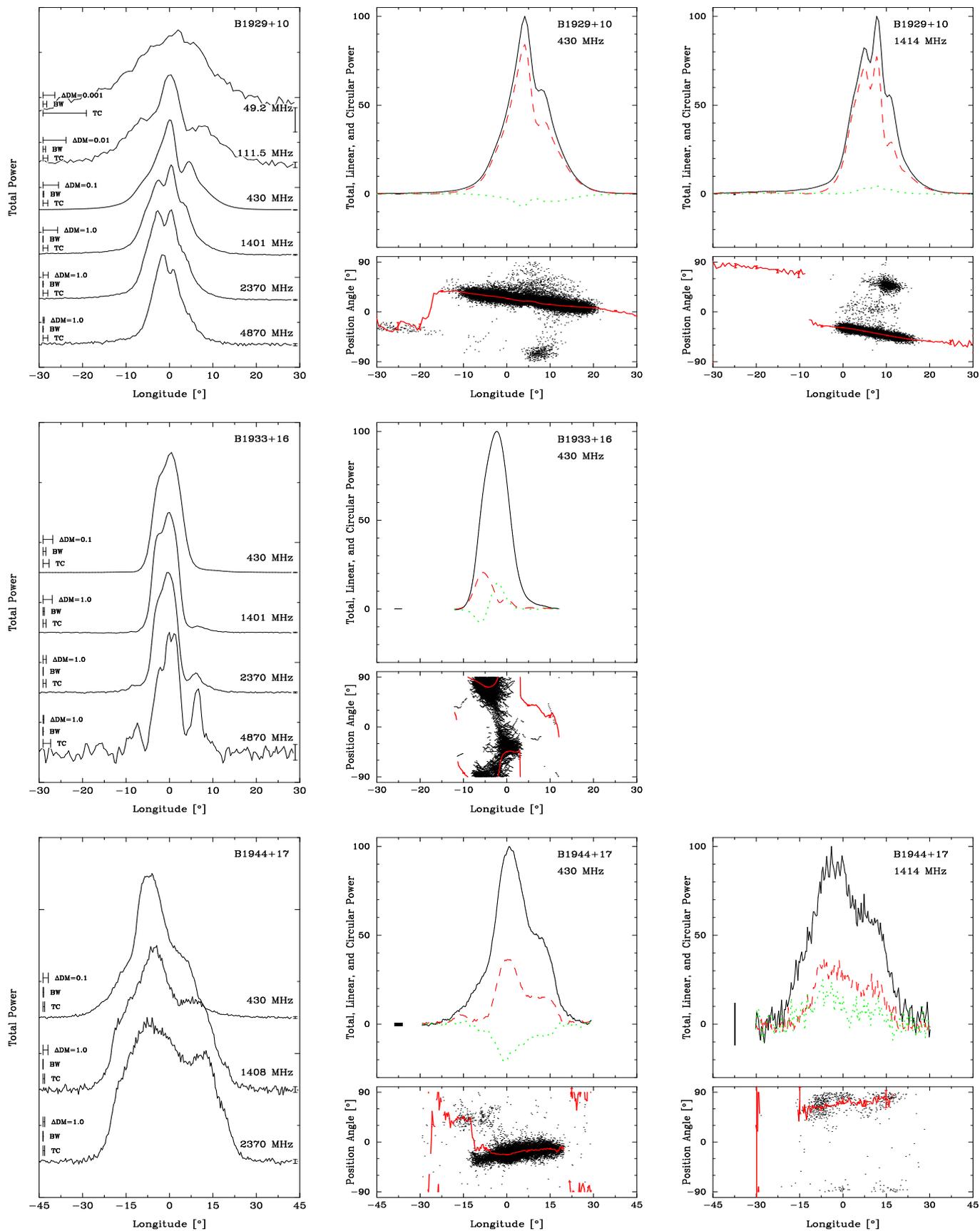
FIG. 12.— Multi-frequency and polarization-histogram displays for B1929+10, B1933+16 and B1944+17 as in Fig. 1. **Center panel credits: RC**
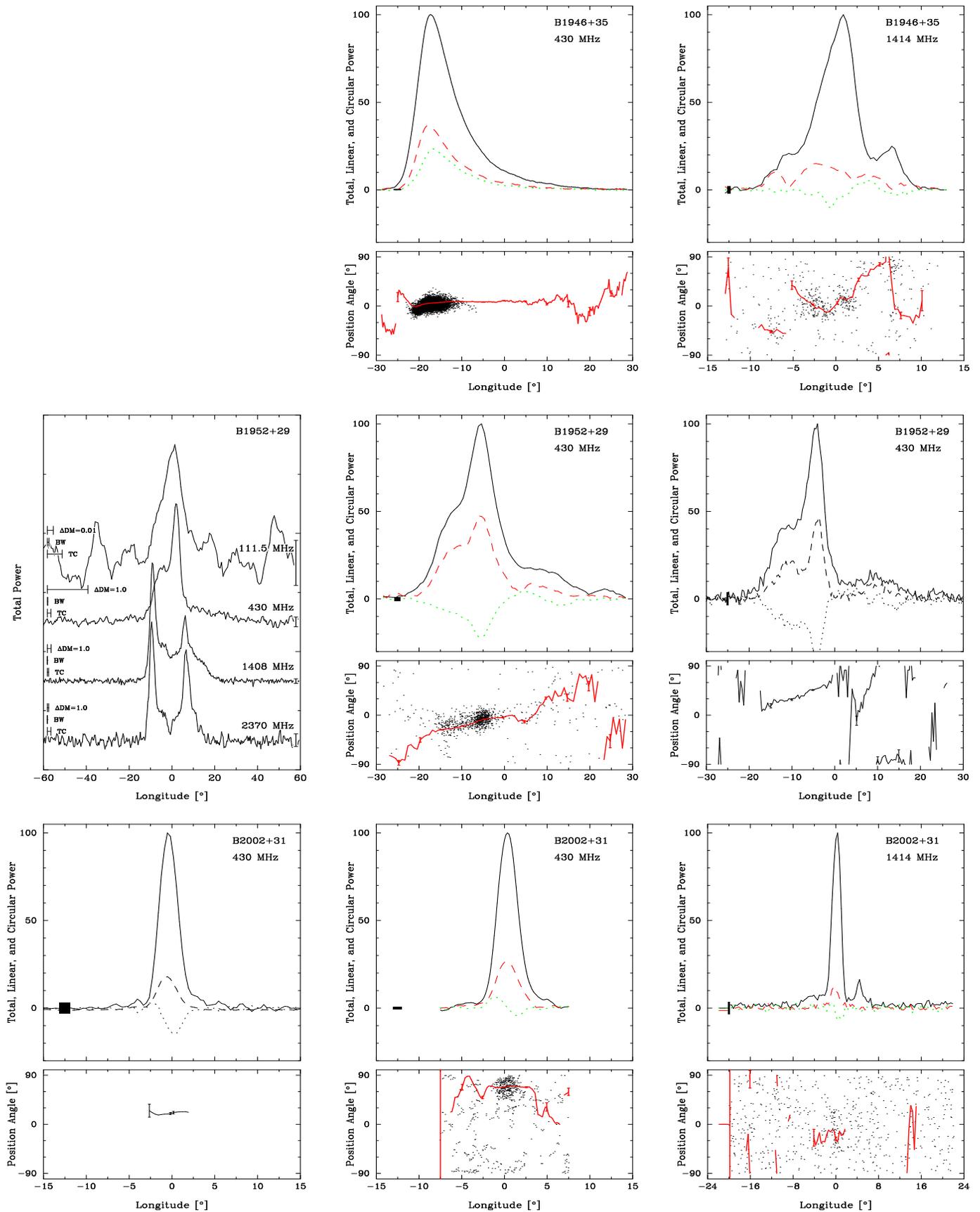
FIG. 13.— Multi-frequency and polarization displays for B1946+35, B1952+29 and B2002+31 as in Fig. 1. **Center panel credits: RC**
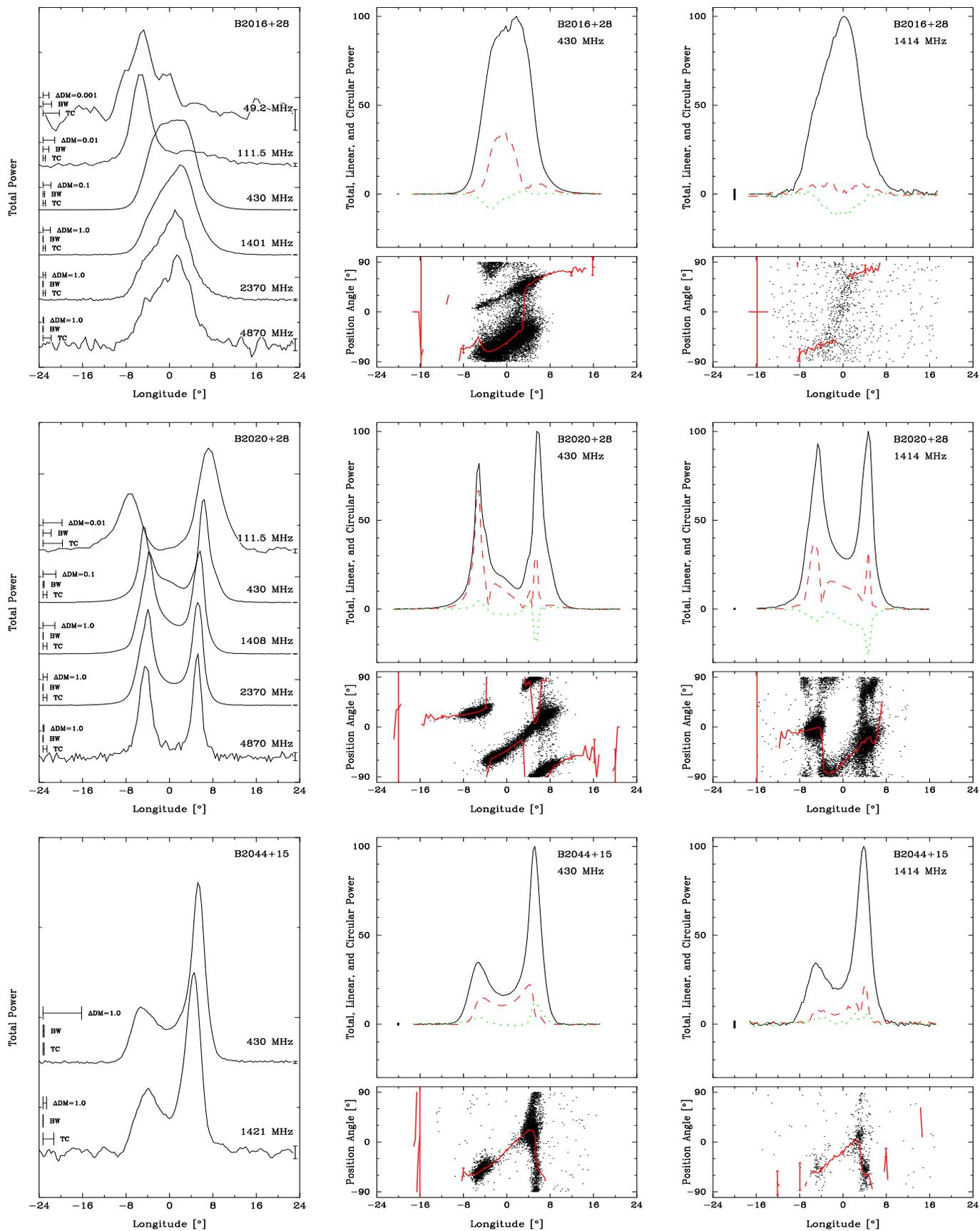
FIG. 14.— Multi-frequency and polarization-histogram displays for B2016+28, B2020+28 and B2044+15 as in Fig. 1.
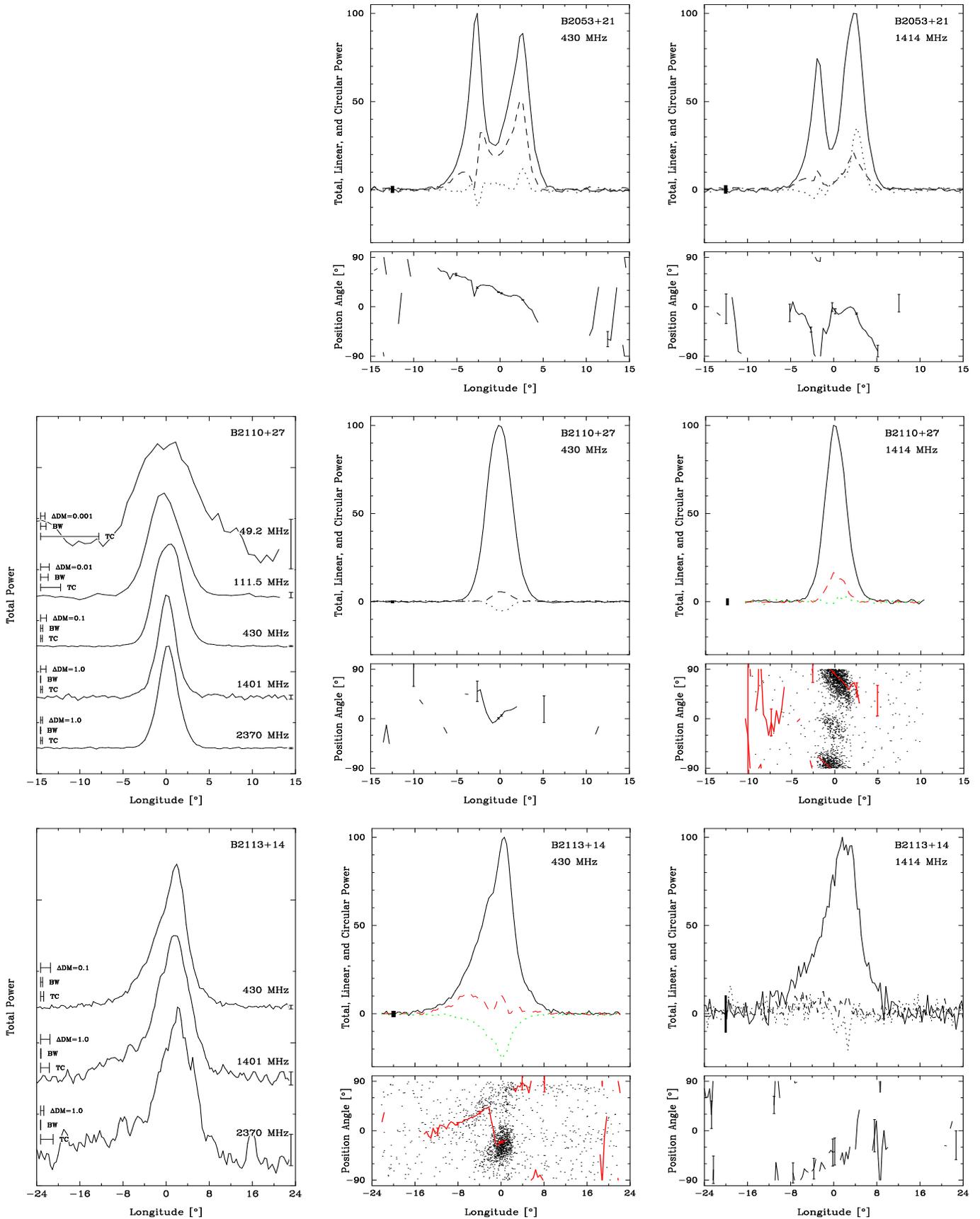
FIG. 15.— Multi-frequency and polarization displays for B2053+21, B2110+27 and B2113+14 as in Fig. 1.
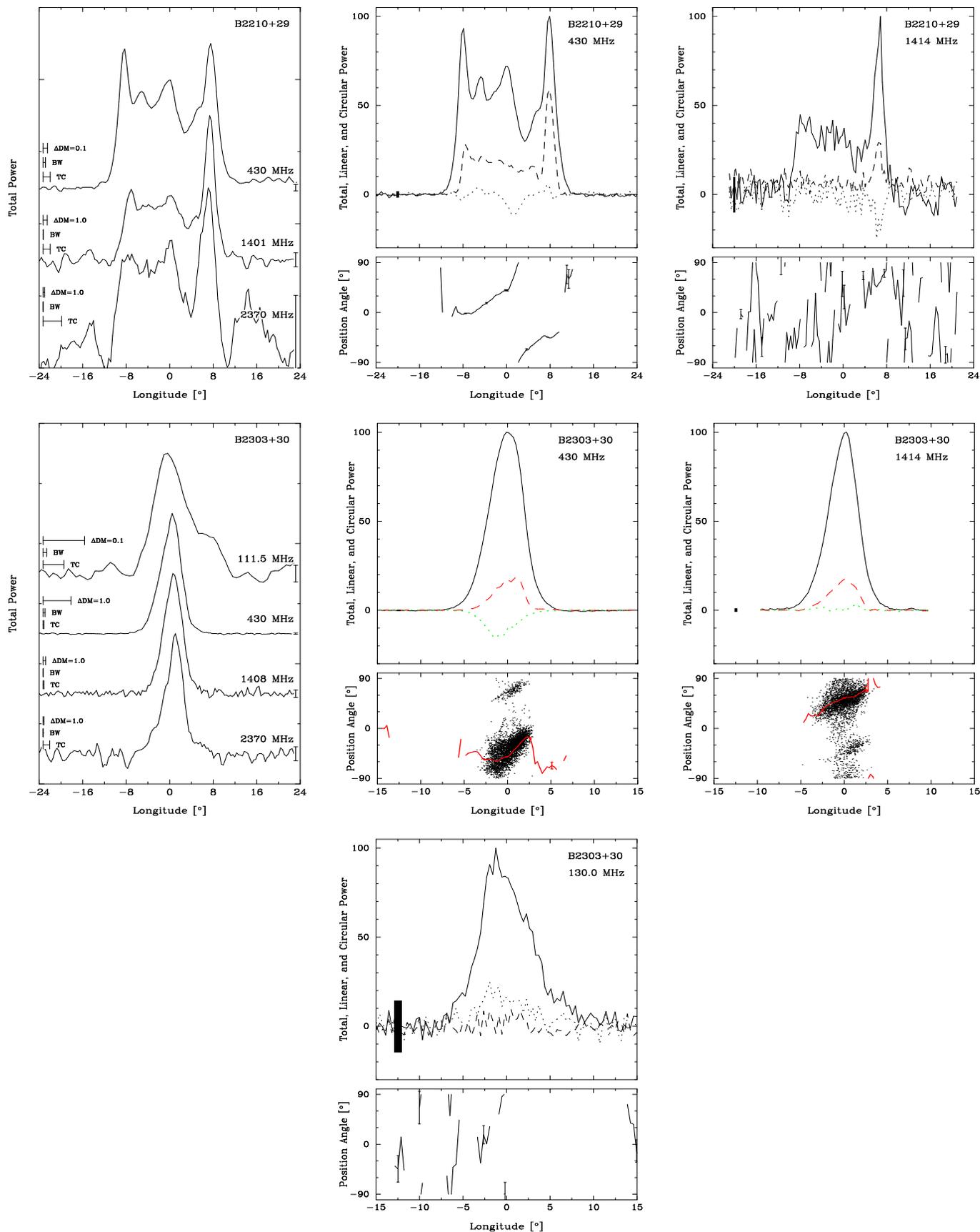
FIG. 16.— Multi-frequency and polarization displays for B2210+29 and B2303+30 as in Fig. 1.
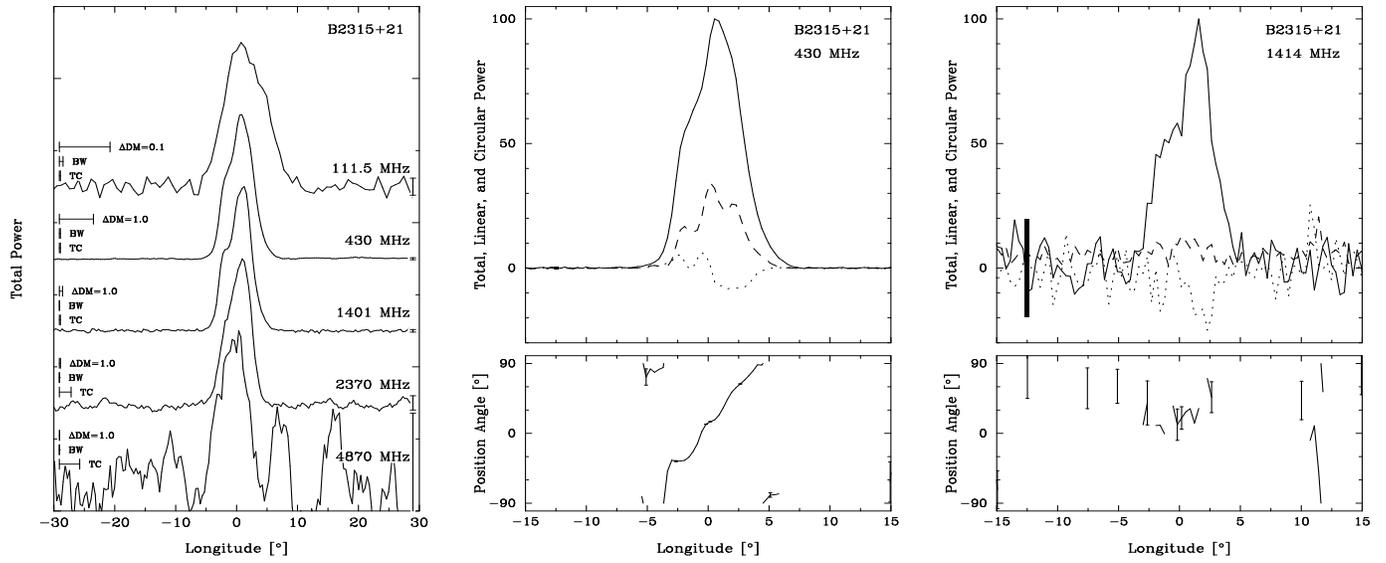
FIG. 17.— Multi-frequency and polarization profiles for B2315+21 as in Fig. 1.
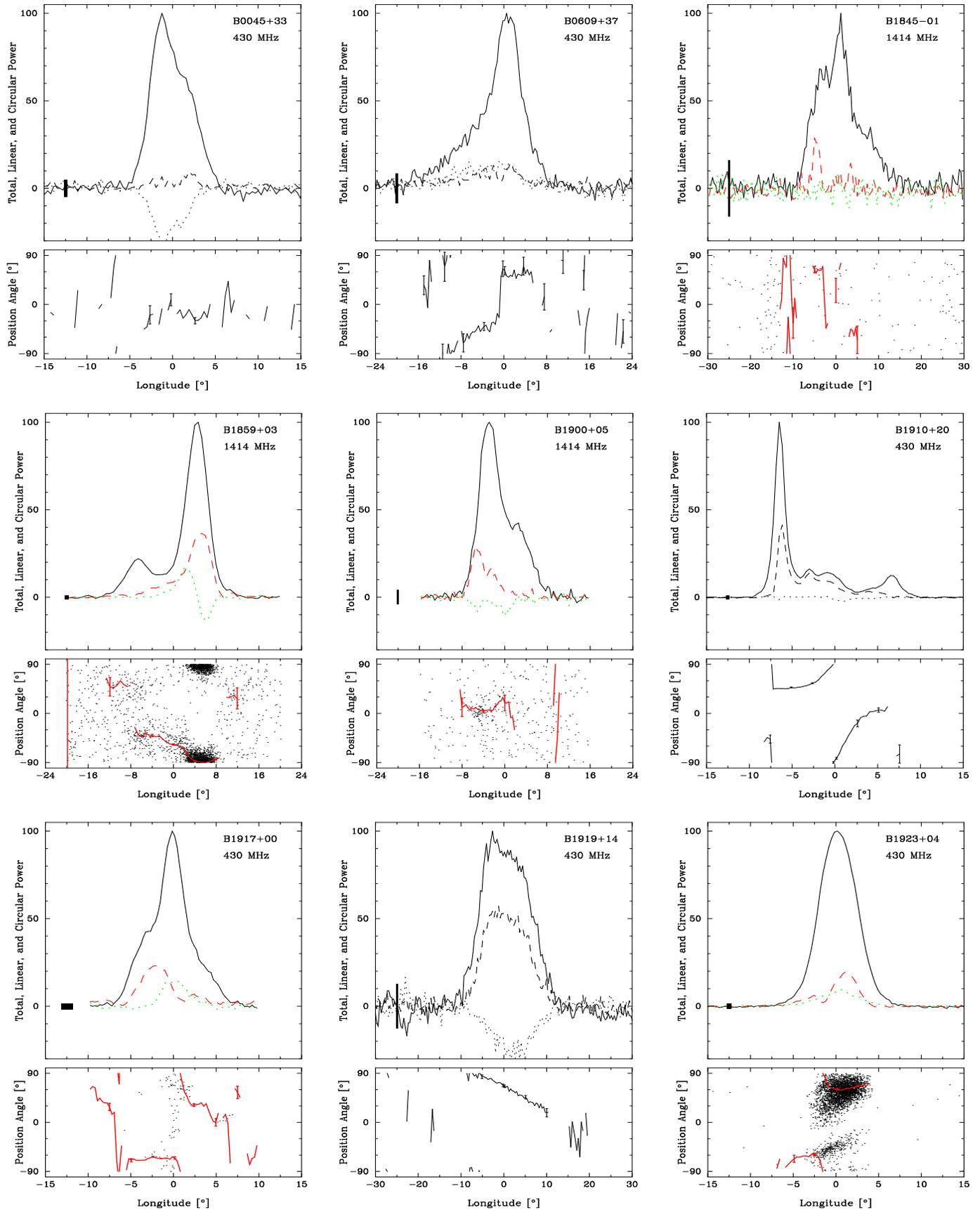
FIG. 18.— Polarization displays for B0045+33 (top left), B0609+37 (top center), B1845−01 (top right), B1859+03 (middle left), B1900+05 (middle center), B1910+20 (middle right), B1917+00 (bottom left), B1919+14 (bottom center) and B1923+04 (bottom right) as in Fig. 1. **Bottom left credit: RC**
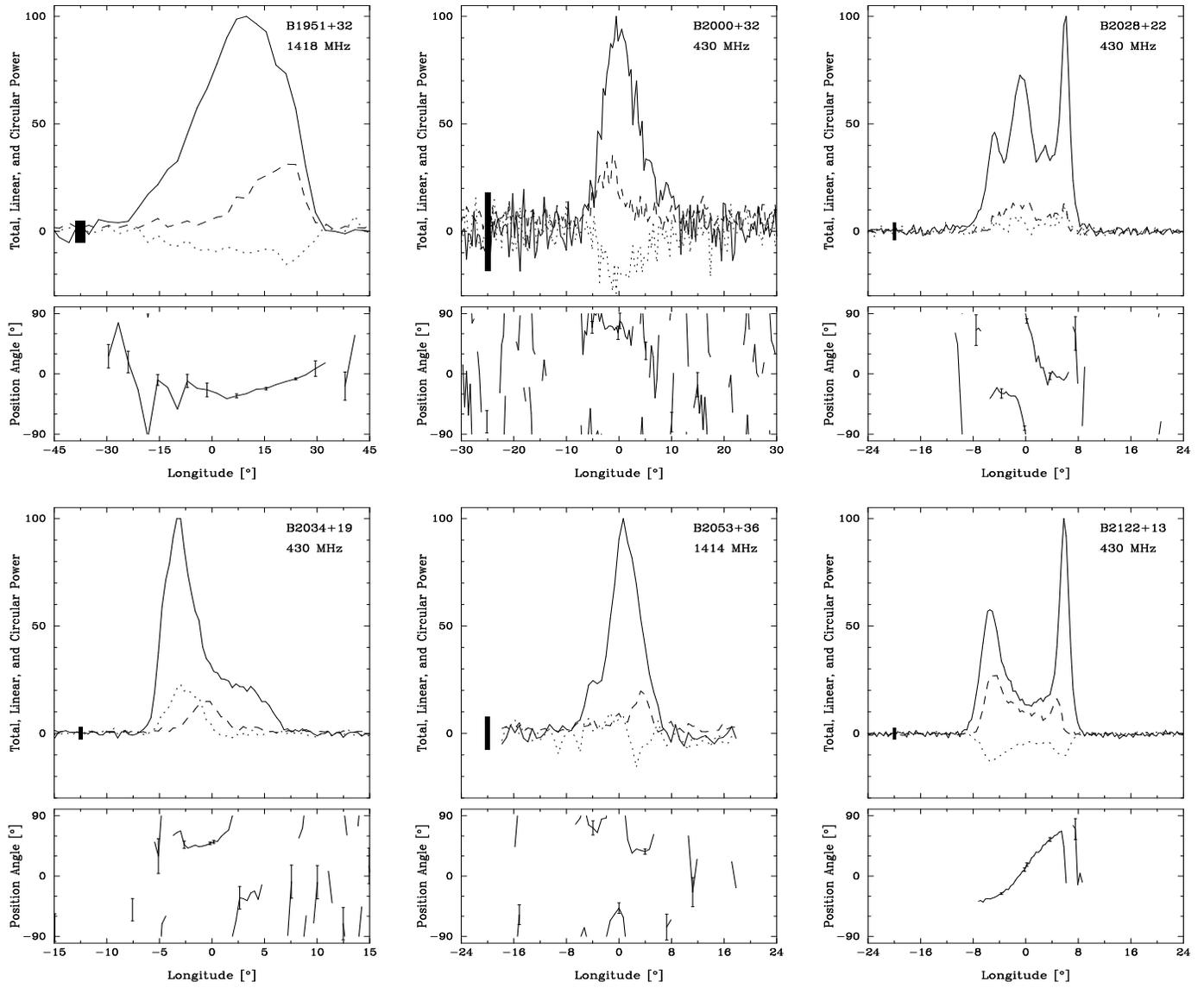
FIG. 19.— Polarization profiles for B1951+32 (top left), B2000+32 (top center), B2028+22 (top right), B2034+19 (middle left), B2053+36 (middle center), and B2122+13 (middle right) as in Fig. 1.

APPENDIX: POLARIMETRIC CALIBRATION

Joanna M. Rankin, N. Rathnasree & Kyriaki Xilouris

While the Arecibo Observatory polarimetric feed systems were known to be imperfect from the 1970s, only slowly were techniques developed to measure these imperfections and ultimately to correct for them. The primary source of this imperfection results from the circumstance that some power is mutually cross-coupled between the two radiometers. At Arecibo in 1992 all of the polarimeter systems involved a pair of nominally left- and right-hand circularly polarized feeds, which were connected to a pair of matched receivers with coherent local oscillators and in turn connected to the Arecibo 40-MHz Correlator, which served as a multiplying polarimeter.

The basic effects of cross-coupling are well described in the Appendix of Stinebring et al. (1984). Indeed, this work reports not only the first technique for measuring the cross-coupling amplitude and phase using pulsar observations, but also shows how these measurements can be used to correct the measured Stokes parameters for the distorting effects of the cross-coupling.

Conceptually, we can understand that the cross-coupled power causes the nominally circularly-polarized feeds to have an elliptically polarized response. In other words, while a purely circularly polarized feed would have the same response to a linearly polarized signal at any orientation (or polarization angle), the ellipticity results in angles of maximum and minimum response 90° apart. In order to understand, then, the behavior of the polarimeter, we need to understand the axial ratio and orientation of the elliptical response of the left- and right-hand feeds.

Our analysis then extends that of the above paper in two significant ways: First, we have made no assumptions about the behavior of the feeds in terms of whether their response was "orthogonal" or "coincident" (see their eqs. A10 and A11), and second we have determined the cross-coupling amplitude and phase as a function of frequency over the entire usable band of the feed.

In order to carry out our analyses, we computed raw Stokes parameters for a pulsar with a region of nearly complete linear polarization; polarized average profiles comprising a few hundred pulses were computed over the full several hours that the pulsar could be tracked in order to obtain the largest possible excursion of parallactic angle. Pulsar B1929+10 has an almost fully polarized leading edge, which is excellent for this purpose as is virtually the entire profile of B0656+14, though the latter is substantially weaker. Then, we recovered the left- and right-hand channel responses $\mathcal{L}$ and $\mathcal{R}$ through use of the Stokes parameter definitions $\mathcal{L} = (I + V)/2$ and $\mathcal{R} = (I - V)/2$. It was then possible to fit sinusoidal curves to the observed dependences of $\mathcal{L}$ and $\mathcal{R}$ as functions of raw instrumental linear polarization angle (rotated with respect to the feed by the changing parallactic angle with hour angle) in order to determine both the axial ratio and the orientation of the cross-coupling-distorted linear response.

This latter fitting procedure is nearly identical to that carried out by Stinebring et al. (1984) in their Fig. 39, except that we fitted to variations in $\mathcal{L}/L$ and $\mathcal{R}/L$ [where the total linear power L is $\sqrt{Q^2 + U^2}$] rather than simply V/L. It is also worth pointing out that these fits are to ratios of polarized intensities, so that any variations in the amplitude of the pulsar signal, due to scintillations or whatever, have no effect on the values, only their uncertainties.

The result then is that the fitted amplitudes determine the axial ratios of the elliptical response (complete circularity would produce no variation with raw feed position angle and imply an axial ratio of unity, whereas a completely linear response would imply an infinite axial ratio); whereas the phase of the variation determines the orientation of the elliptical response relative to the polarization-angle (PA) origin of the polarimeter. In terms of Stinebring et al. (1984), this simple procedure results in the determination of the crucial four parameters, the respective cross-coupling amplitudes ε_1 and ε_2 and the cross-coupling phases ψ_1 and ψ_2 which first appear in their eq. (A2). In particular, these quantities are the only variables upon which the transformation between the intrinsic Stokes parameters and those measured by the imperfect polarimeter depend.

The results of our calibration efforts for the Arecibo 430-MHz line feed and for the 21-cm line feed are given in Figures A.1 and A.2. The left- and right-hand cross-coupling amplitudes are plotted in the top two panels and the left-hand phase in the bottom panel. In fact, we determined both cross-coupling phases and found that they were always orthogonal within our measurement errors, so that only one need be specified. The respective amplitudes, however, appear to exhibit subtle differences, though their overall behavior is very similar in the two cases.

During our October 1992 program observations we obtained several different sets of full-sky tracks on pulsars B1929+10, B0656+14, B1737+13 and B0525+21 as well as shorter tracks from which only the cross-coupling phase could be estimated. B1929+10 provided the most accurate results, and the two feeds appeared stable both from day to day in October 1992 as well as over the interval between several earlier preliminary observations in 1990 January and 1992 March, apart from the overall cross-coupling phase, which we believe results both from differences in our cabling setup for each observation as well (perhaps) as variations in the relative phase of the two receiver channels down from the platform to the control room. Therefore, we were careful to determine the cross-coupling phase for each observation and depend on its stability only over a few hours time.

Apparently, the 21-cm system exhibits a cross-coupling behavior common to many feed systems in use at various observatories—that is, it exhibits minimum cross-coupling amplitudes near the design band center and a progress rise in cross-coupled power toward the band edges. It was then surprising to see that the behavior of the 430-MHz system is very different, with minimum cross-coupled power near the lower band edge at 425 MHz and progressively rising cross-coupled power across the band. Indeed, the level of cross-coupling at the upper band edge is fully 15%, making it absolutely mandatory that observations at this frequency be corrected for the resulting distortion. This also apparently explains a strange phenomenon in our older AO polarimetry: we could not understand for many years why 430-MHz observations of B1929+10 in particular exhibited large variations in fractional circular polarization,
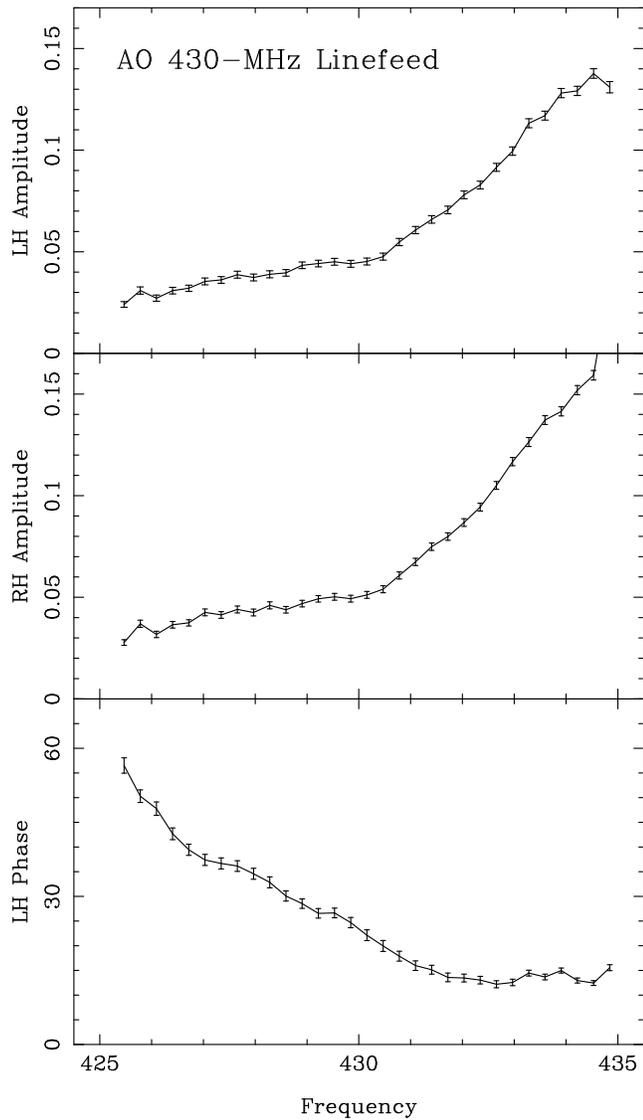
FIG. A.1.— Left- (top panel) and right-hand (middle panel) cross-coupling amplitudes and the left-hand cross-coupling phase (bottom panel) as a function of frequency for the Arecibo Observatory 430-MHz line feed as determined from a full-sky track of pulsar B1929+10 in October 1992. The right-hand phase is orthogonal to the plotted left-hand phase within the observational errors, which represent one standard deviation.
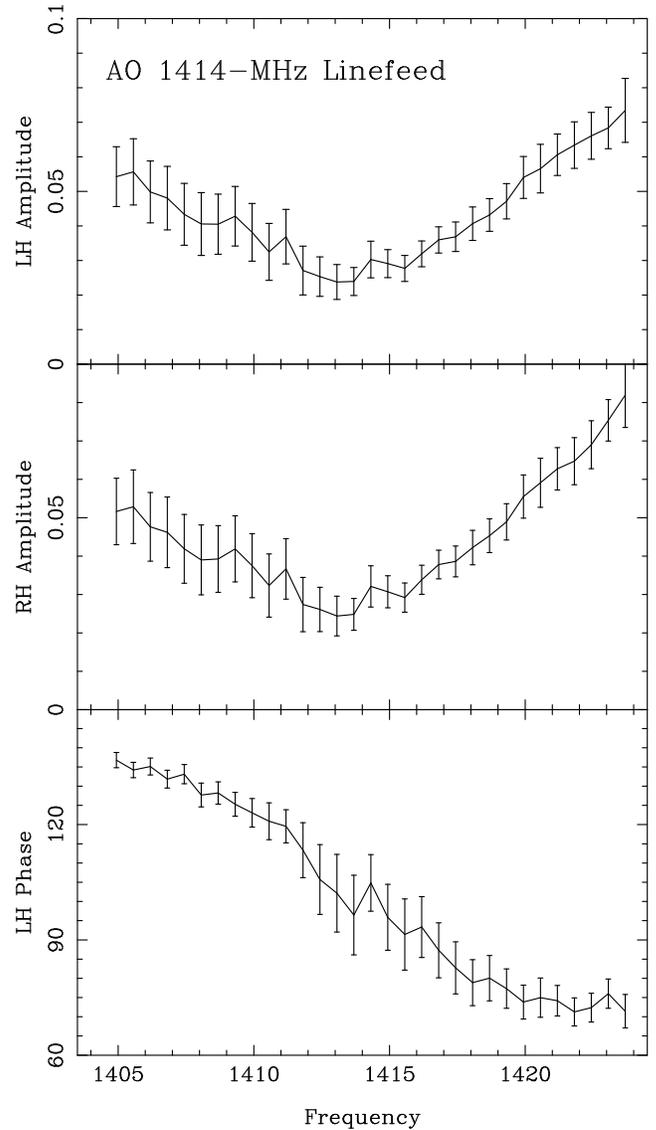

FIG. A.2.— Cross-coupling amplitudes and phase for the Arecibo Observatory 21-cm line feed, determined from a full-sky track of pulsar B1929+10 in October 1992, as in Fig. A1.

between essentially zero and almost 40%. The reason we can now see is almost certainly that for such a low dispersion pulsar, the fractional circular would vary greatly depending upon how the scintillation-produced spectral variations excited the feed! More highly dispersed stars tend to have more bright scintiles within our passband, and thus the cross-coupling distortion tended to average across them.

Finally, we used the above cross-coupling information to correct the measured Stokes parameters whenever possible. If we write eq. (A5) of Stinebring *et al.* (1984) as $\mathbf{S'} = \mathbf{MS}$, where $\mathbf{S}$ is the true Stokes vector $\mathbf{S'}$ the measured one, and $\mathbf{M}$ is the 4×4 Müller matrix relating the two, then our correction of the Stokes parameters took the form

$$\mathbf{S}(f) = \mathbf{M^{-1}}[\varepsilon_1(f), \varepsilon_2(f), \psi_1(f), \psi_1(f) \pm 90°]\mathbf{S'}(f). \quad (1)$$

Despite these careful efforts, our calibrations vary considerably in quality. The great bulk of the 430- and 1400-MHz observations were fully calibrated both in terms of standard-source observations to determine the relative left- and right-hand channel gains as well as the cross-coupling distortion corrections outlined above. However, in some cases the standard-source pointings were corrupted by interference, and in a few cases, our shorter trackings to determine ψ_1 were unsuccessful. We note these faults in Tables 2 & 3 above.